Journal of
Medicinal Chemistry

Article

Proteolysis Targeting Chimeras for the selective degradation of Mcl-1/Bcl-2 derived from nonselective target binding ligands

Ziqian Wang, Nianzhe He, Zongwei Guo, Cuili Niu, Ting Song, Yafei Guo, Keke Cao, Anhui Wang, Junjie Zhu, Xiaodong Zhang, and Zhichao Zhang

J. Med. Chem., **Just Accepted Manuscript** • DOI: 10.1021/acs.jmedchem.9b00919 • Publication Date (Web): 07 Aug 2019

Just Accepted

is published by the American Chemical Society. 1155 Sixteenth Street N.W., Washington, DC 20036

Proteolysis Targeting Chimeras for the selective degradation of Mcl-1/Bcl-2 derived from nonselective target binding ligands

*Ziqian Wang,[a] Nianzhe He,[a] Zongwei Guo,[b] Cuili Niu,[a] Ting Song,[a] Yafei Guo,[b] Keke Cao,[b] Anhui Wang,[a] Junjie Zhu,[a] Xiaodong Zhang [a] and Zhichao Zhang [a]**

[a]State Key Laboratory of Fine Chemicals, Zhang Dayu School of Chemistry, Dalian University of Technology, Dalian, Liaoning (China), 116024.

[b]School of Life Science and Technology, Dalian University of Technology, Dalian, Liaoning (China), 116024.

KEYWORDS: Proteolysis Targeting Chimeras; protein-protein interaction; Bcl-2 family protein; linker; selectivity

Abstract

Proteolysis Targeting Chimera (PROTAC) recruits an E3 ligase to a target protein to induce its ubiquitination and subsequent degradation. We reported the success in the development of two PROTACs (**C3** and **C5**) that potently and selectively induce the degradation of Mcl-1 and Bcl-2 (DC_{50} = 0.7 and 3.0 μM), respectively, by introducing the E3 ligase cereblon (CRBN)-binding ligand pomalidomide to Mcl-1/Bcl-2 dual inhibitors **S1-6** and **Nap-1** with μM-range affinity. **C3**-induced Mcl-1 ubiquitination translated into much more lethality in Mcl-1-dependent H23 cells than the most potent Mcl-1 occupancy-based inhibitor **A-1210477** with nM-range affinity. Moreover, structure-activity relationship (SAR) analysis and molecular dynamic (MD) simulations discovered the structural basis for turning nonselective or promiscuous Bcl-2 family ligands into selective PROTACs. **C3** and **C5** exhibited reversible depletion in living cells, which provides a new potent toolkit for gain-of-function studies to probe the dynamic roles of Bcl-2 and Mcl-1 in apoptosis networks.

Introduction

Occupancy-based pharmaceutical strategies need high local inhibitory percentages (usually 90-95 %) of disease-related proteins, which is necessary to assure therapeutic efficacy[1-2]. Therefore, a heavy burden has been imposed on developing high-affinity small molecule ligands, which is always forlorn for targets mediating protein-protein interactions (PPIs).

The recent development of Proteolysis Targeting Chimeras (PROTACs), which comprise a ligand binding an E3 ubiquitin ligase conjugated to a small molecule warhead binding the target protein, offer a new pharmacological strategy to solve these limitations[1-5]. PROTACs trigger target ubiquitination and subsequent proteasomal degradation by recruiting targets into spatial proximity with E3 ubiquitin ligases[1-7]. Thus, PROTACs can act at substoichiometric occupancies for the targets in a catalytic mechanism, do not require excessive drug concentrations to ensure occupancy-based inhibition and can avoid adverse side effects[8,9].

To date, PROTACs have succeeded in degrading kinases[10-15], bromodomains and extra-terminal (BET) proteins[16-20], and hormone receptors[21,22] by using warheads that show nanomolar affinity for these targets. However, PROTACs for α-helix-mediated PPI target degradation are still rare[23-25]. One of the major challenges is that binding ligands for these PPI targets are usually large hydrophobic molecules (Mw > 800 and LogP > 5), as they are required to make discontinuous, noncovalent contacts over a large and flat binding surface area (>800 Å^2)[26-28]. Therefore, it is difficult for PROTACs obtained by conjugating these PPI inhibitors with a hydrophobic E3 ligase ligand (Mw > 250)[1-5] via an alkyl or PEG linker (usually Mw = 100-200)[1-5] to exhibit acceptable solubility and membrane permeability.

Nevertheless, PPIs are involved in most cellular processes, including differentiation, apoptosis, signal transduction and transcription[29]. Therefore, the modulation of PPIs is considered as a promising strategy toward next-generation therapeutics[27-29]. For example,

Bcl-2 family proteins play essential roles in the regulation of intrinsic apoptosis via α-helix-mediated PPIs between pro- and anti-apoptotic members[30-32]. Anti-apoptotic proteins, which are represented by Mcl-1 and Bcl-2, are considered as attractive targets for potential cancer treatments[33].

Recently, researchers have demonstrated that the basis of degradation efficiency rely on protein-protein interactions between the E3 ubiquitin ligase and the target protein, rather than the binding affinity of ligands[34,35]. Therefore, the potent and selective PROTACs for degrading PPI targets can be developed using target binding ligands with relative lower Mw via modulating the length and conformation of the linkers to compensate for the low-affinity of ligands, leading to a dramatic enhancement of target protein removal.

In this article, we constructed two series of PROTACs, **H1-H5** and **C1-C6**, by introducing the E3 ligase cereblon (CRBN)-binding ligand pomalidomide to Bcl-2/Mcl-1 dual inhibitors **S1-6**[36-38] and **Nap-1**[39] (Fig. 1a), which exhibits a lower Mw (approximately 500) and a lower binding affinity for both targets in the μM-range, via alkyl and PEG linkers of different lengths. Among them, PROTACs **C3** and **C5** were observed to potently and selectively induce the ubiquitination and proteasomal degradation of Mcl-1 and Bcl-2 *in cellulo*, respectively, by hijacking a CRBN ubiquitin ligase to form a ternary complex with the target protein. Moreover, structure-activity relationship (SAR) analysis and molecular dynamic (MD) simulations in a certain extent revealed the structural basis for turning nonselective or promiscuous Bcl-2 family ligands into more selective degraders by changing the length and conformation of their linkers, which is valuable for the design of other PROTACs. Moreover, **C3** and **C5** exhibited reversible depletion in living cells, which provides a new potent toolkit for gain-of-function studies to probe the dynamic roles of Bcl-2 and Mcl-1 in apoptosis networks.

Results and Discussion

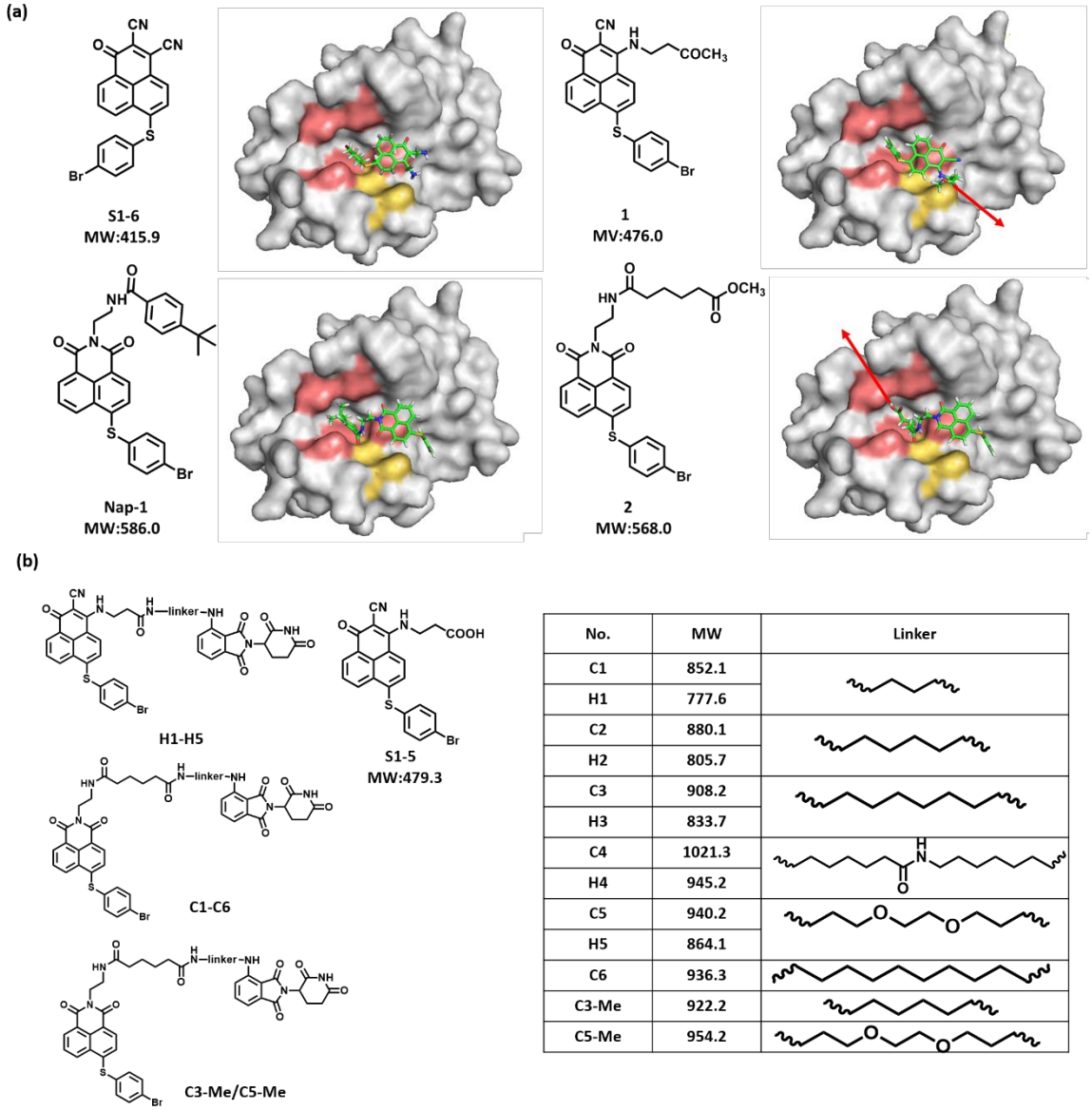

No.	MW	Linker
C1	852.1	
H1	777.6	
C2	880.1	
H2	805.7	
C3	908.2	
H3	833.7	
C4	1021.3	
H4	945.2	
C5	940.2	
H5	864.1	
C6	936.3	
C3-Me	922.2	
C5-Me	954.2	

Figure 1. (a) Chemical structures, molecular weights and NMR-derived binding mode of the parent inhibitors **S1-6** (top, left), **Nap-1** (bottom, left) and intermediates **1** (top, right), **2** (bottom, right) in complex with Mcl-1 (PDB ID: 2NLA). The pink and yellow surface highlight p2 and p3 binding pockets, and red arrows highlight exit vectors for linking. (b) Chemical structures and molecular weights of **H1-H5**, **C1-C6**, **C3-Me**, **C5-Me** and **S1-5**.

Herein, we selected two Bcl-2 family inhibitors, **S1-6** and **Nap-1** (Fig. 1a), whose

opposite binding orientations to the BH3 groove of Bcl-2 proteins have been identified by 2D and 3D NMR in our previous studies[36-39]. For **S1-6**, the solvent exposed 3-cyano group located in the P3 pocket of the BH3 groove provides a suitable point for linker attachment without tethering the binding properties (Fig. 1b, top). We then replaced the cyano group with the 3-aminopropanoic acid methyl ester group, which yielded compound 1 (Fig. 1a). For **Nap-1** (Fig. 1b, bottom), the 4-tert-butylbenzoic acid group bond to the P2 pocket was replaced by hydrophobic alkyl chains for further linker connection, yielding compound 2 (Fig. 1a).

To evaluate the effects of distance and spatial location between the ligands and the E3 ligase, five different linkers of varying composition and length were attached to 1 and 2 via amide bond formation. Finally, the CRBN binding ligand pomalidomide was attached, yielding PROTACs **H1-H5** and **C1-C6** (Fig. 1c).

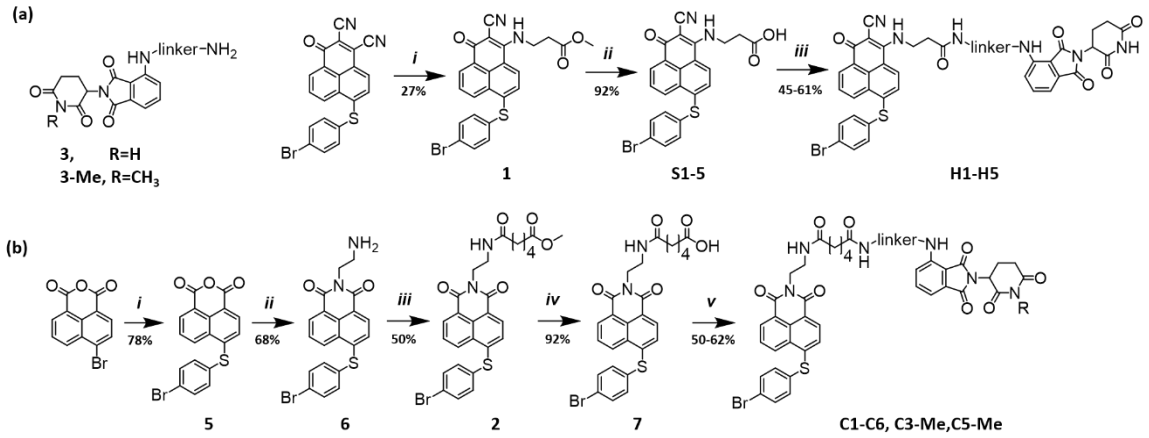

Scheme 1. Synthesis routes of **1**, **2**, **H1-H5**, **C1-C6**, **C3-Me** and **C5-Me**. (a) Reaction conditions: *i*) methyl 3-aminopropanoate hydrochloride, NaOH, CH_3CN/H_2O, rt; *ii*) NaOH, THF/H_2O, rt; *iii)* **3**, DIEA, HATU, DCM, rt. (b) Reaction conditions: *i*) 4-Bromothiopheno, NEt_3, DMF, reflux; *ii*) ethylenediamine, NEt_3, EtOH, reflux; *iii*) 6-Methoxy-6-oxohexanoic acid, DIEA, HATU, DCM, rt; *iv*) NaOH, THF/H_2O, rt; *v*) **3/3-Me**, DIEA, HATU, DCM, rt.

To achieve the desired ligands, a generally applicable three-step synthetic strategy was devised (Scheme 1). First, intermediate compounds **1** and **2** were synthesized according to earlier reported routes[36-39]. Second, the linkers bearing a free amine group at one end and a Boc-protected amine group at the other end were attached to the pomalidomide via S_{NAr} reactions[40]. In the third step, deprotection of the Boc-protected amine and subsequent HATU-mediated amide bond formation with the carboxylic acid in intermediate molecules **1** and **2** afforded the desired PROTAC compounds, respectively.

Table 1. Binding affinities of **S1-6**, **Nap-1**, intermediates **1**, **2**, **C1-C5** and **H1-H5** with Bcl-2 and Mcl-1 determined by ELISA, data are expressed as the mean ± s.e.m.

Compounds	**IC_{50} (μM)**	
	Mcl-1	**Bcl-2**
S1-6	2.03 ± 1.02	2.31 ± 0.87
Nap-1	4.45 ± 1.53	3.18 ± 1.39
1	3.46 ± 0.94	4.52 ± 1.28
2	5.95 ± 1.49	4.78 ± 2.06
C1	7.89 ± 2.47	15.21 ± 4.33
C2	1.51 ± 0.39	10.02 ± 2.90
C3	0.78 ± 0.12	0.54 ± 0.27
C4	15.12 ± 3.85	13.47 ± 4.57
C5	11.81 ± 2.48	4.94 ± 1.36
C6	5.40 ± 1.25	7.66 ± 2.28
H1	10.64 ± 4.19	10.48 ± 3.66

H2	9.95 ± 2.72	9.71 ± 2.13
H3	7.65 ± 2.56	1.94 ± 0.58
H4	16.01 ± 4.88	11.65 ± 4.44
H5	2.29 ± 1.33	2.24 ± 0.89

Enzyme-linked immunosorbent assay (ELISA) experiments were performed to measure the binding abilities of the PROTAC molecules toward Mcl-1 and Bcl-2 (Table 1 and Fig. S1). Compared with the parent inhibitors **S1-6** and **Nap-1**, intermediate molecules **1**, **2** and PROTACs **C1-C6** and **H1-H5** showed similar overall binding affinities in the μM range with Mcl-1 and Bcl-2, denoting that the binding modes were still conserved.

To assess the extent of PROTAC-mediated protein removal, we analyzed the protein levels of Mcl-1 and Bcl-2 after a 12 h treatment with **C1-C6** or **H1-H5** by immunoblotting in Hela cancer cells. Hela cells were chosen because they are less susceptible to the cytotoxic effects of Bcl-2 family protein knockdown or inhibition. The parent inhibitors **S1-6** and **Nap-1** were included as controls (Fig. 2). No significant depletion in Mcl-1 or Bcl-2 was observed in Hela cells upon treatment with 10 μM PROTACs **H1-H5** (< 20 %), and Mcl-1 levels increased beyond the vehicle control levels in some cases, which suggested that **H1-H5** function more as protein inhibitors than as degraders due to the Mcl-1 upregulation under inhibition stress. The bands at high mass in addition of H4 and H5 were not ubiquitin adducts of Mcl-1 (Fig. S2). In contrast, PROTACs **C3** and **C5** induced a marked concentration-dependent depletion of Mcl-1 and Bcl-2, respectively. Compound **C3** selectively induced a 70 % decrease in Mcl-1 levels at 1 μM and progressively downregulated it to less than 10 % at 10 μM. In contrast, Bcl-2 protein was not depleted, even upon treatment with 10 μM **C3**. In comparison, **C5** served as a selective Bcl-2 reducer that reduced protein levels progressively from 10 % to 90 % as the dose increased from 1 to 10 μM. As a control, the parent inhibitors **Nap-1** and **S1-6** showed no depletion of either

Mcl-1 or Bcl-2 at 10 μM.

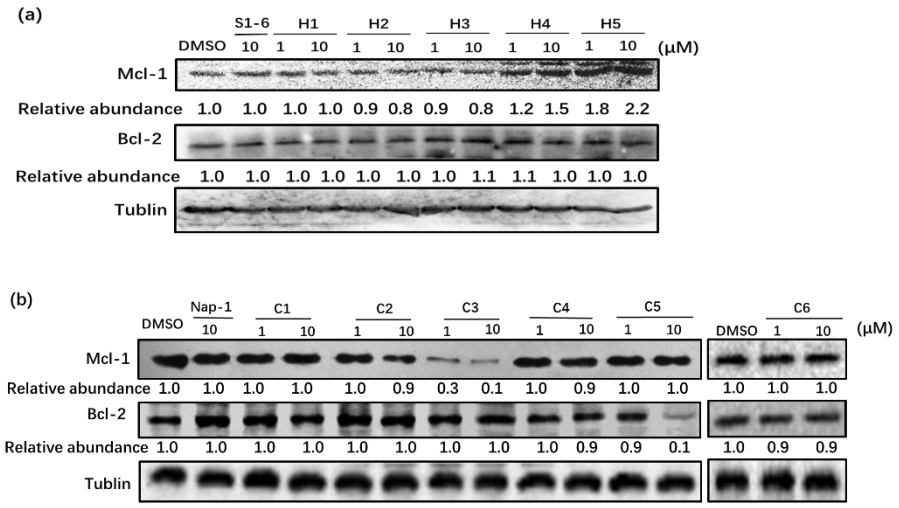

Figure 2. PROTACs downregulated the protein levels of their respective targets. Mcl-1 and Bcl-2 protein levels were analyzed by Western blotting in Hela cells treated with (a) **H1-H5** and (b) **C1-C6** for 12 h. All western blot figures represent the results from n = 3 independent samples.

Consequently, time- and dose-dependent depletion of Mcl-1/Bcl-2 by **C3** and **C5** were tested (Fig. 3 and Fig. S3,S4). Our previously reported Mcl-1 degrader, **S1-5**[38] (Fig. 1a), was added as a control. **S1-5** could form hydrogen bonds with His224 from Mcl-1 to drive a helical QRN conformation and finally lead to the degradation of Mcl-1 by benefiting from its binding ability to the E3 ligase Mule. As shown in Fig. 3a and Fig. S3, Mcl-1/Bcl-2 levels in Hela cells were monitored over a 24-hour time course upon treatment with 10 μM of compounds **C3**, **C5** and **S1-5**. Progressive removal of Bcl-2 family proteins over time was observed for the three compounds, but with different selectivity and efficiency. Ten micromolar **C3** began to markedly deplete Mcl-1 at 8 h and reached the maximal reduction at 12 h, when approximately 80 % of the protein had been removed. After that, Mcl-1 recovery occurred probably owing to the possibility of compound instability, for the

mRNA level over 0-24 h (Fig. S5). In contrast, Bcl-2 remained constant during the time course. For **C5**, remarkable Bcl-2 but not Mcl-1 depletion was observed at 2 h, and almost all the Bcl-2 proteins were depleted after 12 h of treatment. Bcl-2 abundance also recovered after 16 h. For **S1-5**, selective depletion of Mcl-1 was observed at 12 h and 80 % of Mcl-1 was depleted at 24 h. Reassuringly, all these compounds exhibited dose-dependent and selective depletion activities (Fig. 3b and Fig. S4). Compound **C3** exhibited Mcl-1 removal activity with a DC_{50} value of 0.7 μM, while the DC_{50} value of **C5** against Bcl-2 was 3.0 μM at 12 h. The DC_{50} value of **S1-5** for Mcl-1 was much higher than that of **C3**, which was 3.6 μM. The much more efficient Mcl-1 depletion induced by **C3** than **S1-5** was further verified in K562 cells (Fig. S6).

Interestingly, compared with ELISA data, we found an inconsistency between binding affinity and degradation potency, and, more importantly, the degradation selectivity. For example, even though all 10 PROTACs (**C1-C6** and **H1-H5**) exhibited a similar μM binding affinity to Mcl-1 and Bcl-2, only **C3** and **C5** degraded Mcl-1 and Bcl-2, respectively, which demonstrated that potency and selectivity of the PROTACs can be optimized via modulating the length and conformation of the linkers.

To evaluate the specificity of **C3**/**C5**-induced degradation, we tested the protein level of another of Bcl-2 family member, Bcl-xl, and the potential off-targets of some Bcl-2 family inhibitors (MDM2 and tubulin)[39,41], which has been reported by our group. None of these protein levels decreased upon addition of 10 μM **C3** or **C5**, further validated the specificity of **C3**/**C5**-induced Mcl-1/Bcl-2 degradation (Fig. S7).

Despite proving selective degradation within the Bcl-2 family members and some potential off-targets of Bcl-2 family inhibitors, we cannot exclude the degradation of unrelated targets in the global proteome. Therefore, a global proteomic experiment would help assess the potential efficacy and safety risks of drug discovery program in the future.

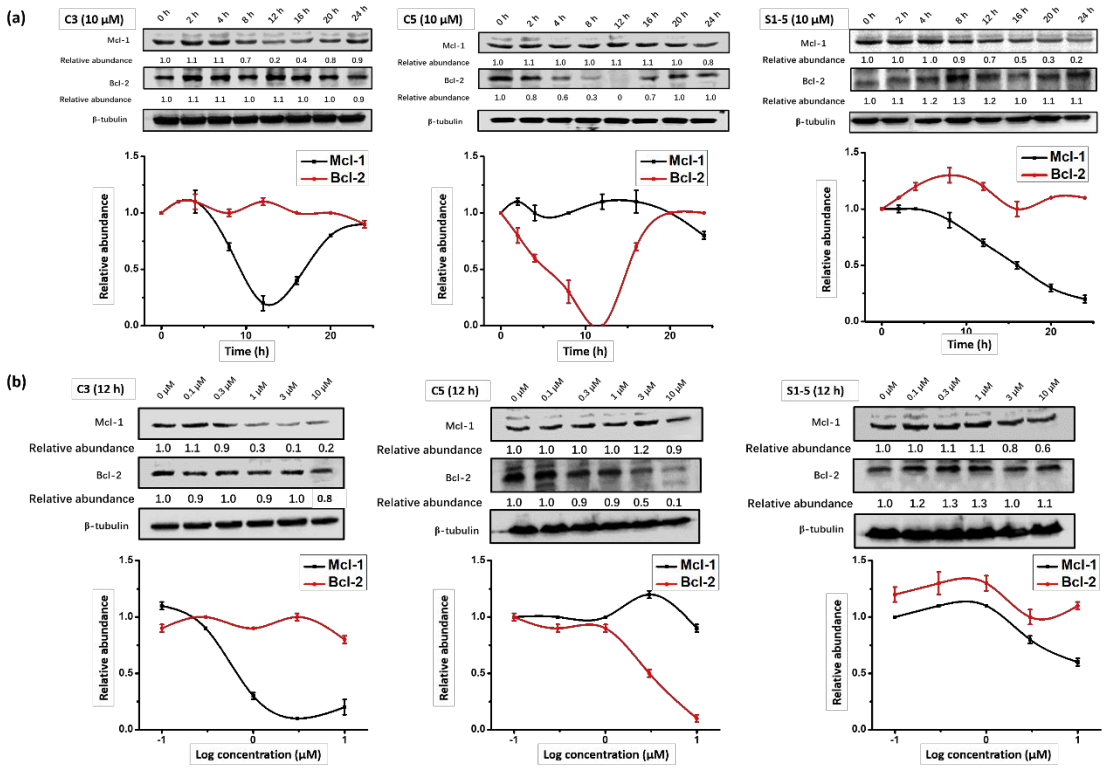

Figure 3. PROTACs induced time- and concentration-dependent selective depletion of Mcl-1 or Bcl-2 protein in Hela cells. Protein levels were visualized by immunoblotting and quantified relative to the DMSO control. (a) Protein levels after treatment with 10 μM **C3, C5** or **S1-5** over a 0-24 h time gradient. (b) Protein levels after treatment with a 0-10 μM concentration gradient of **C3**, **C5** or **S1-5** for 12 h. All western blot figures represent the results from n = 3 independent samples, the replicates are shown as Fig. S3, S4 in SI. Error bars show mean ± s.d. (n=3).

Next, we determined the mechanism of the PROTAC-mediated Mcl-1/Bcl-2 degradation. First, replacing the pomalidomide in **C3** and **C5** with N-methylated glutarimide, which yields **C3-Me** and **C5-Me** (Fig. 1b, for synthesis route see Scheme 1b), abolished their capability of inducing Mcl-1/Bcl-2 degradation (Fig. 4a,b). Simultaneously, pretreatment with the proteasome inhibitor **MG-132**, the parent Bcl-2 inhibitor **Nap-1** and the CRBN inhibitor pomalidomide effectively blocked both **C3**-induced Mcl-1 depletion (Fig. 4a) and

C5-induced Bcl-2 depletion (Fig. 4b). Second, a CRBN pull-down assay was performed to trap potential ternary complex members in the presence of PROTAC by co-immunoprecipitation. When a whole-cell lysate from Hela cells was incubated with different concentrations of compounds **C3** or **C5**, selective interactions between Mcl-1 or Bcl-2 with CRBN and dose-dependent CRBN recruitment were detected (Fig. 4c), consistent with their degrading selectivity. In contrast, no interactions between either Mcl-1 or Bcl-2 with CRBN were detected upon addition of the invalid PROTAC **H3** (Fig. S8). All together, these data provided clear evidence that **C3** and **C5** mediated target protein degradation in a bona fide PROTAC-based mechanism, in which the degrading potency and selectivity was dependent on a ternary complex comprised of the target protein, PROTAC, and CRBN.

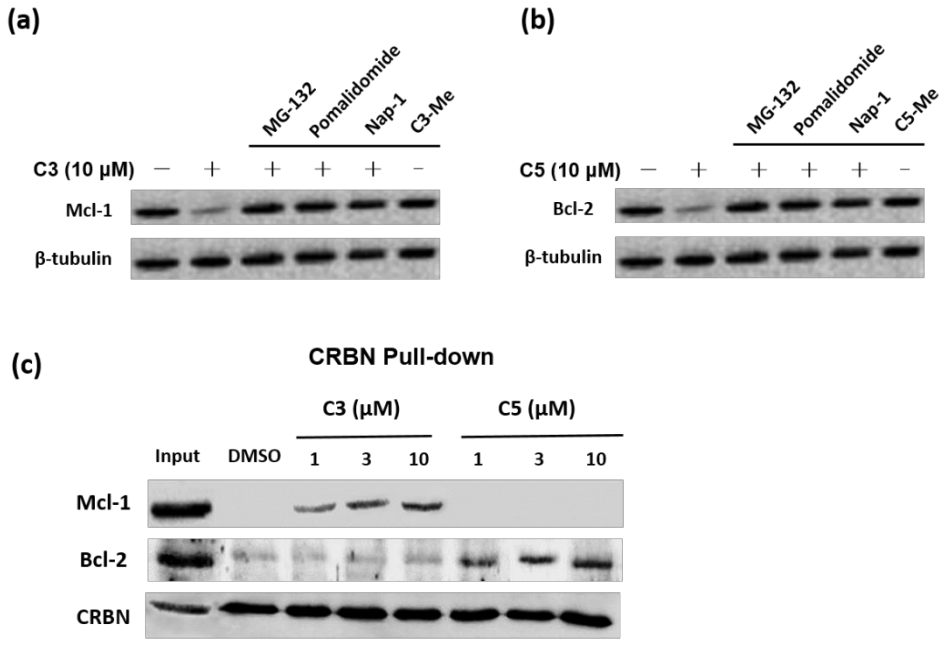

Figure 4. The stable ternary complexes between Mcl-1/Bcl-2, CRBN and the PROTACs are required for the superstoichiometric ubiquitination and degradation of target proteins. (a,b) Immunoblot for Mcl-1 (a) or Bcl-2 (b) after pretreatment with 50 μM **MG132**, 50 μM pomalidomide or 50 μM **Nap-1**, followed by PROTAC treatment (10 μM **C3** or **C5**) in

Hela cells. (c) Stable interactions between Mcl-1/Bcl-2 and CRBN were induced by the addition of the PROTACs in Hela cells. Immobilized CRBN was used as a bait to trap Mcl-1 and Bcl-2 in the presence of a concentration gradient of **C3** or **C5**. Protein levels of the trapped proteins were visualized by immunobloting in the pull-down reactions. All western blot figures represent the results from n = 3 independent samples.

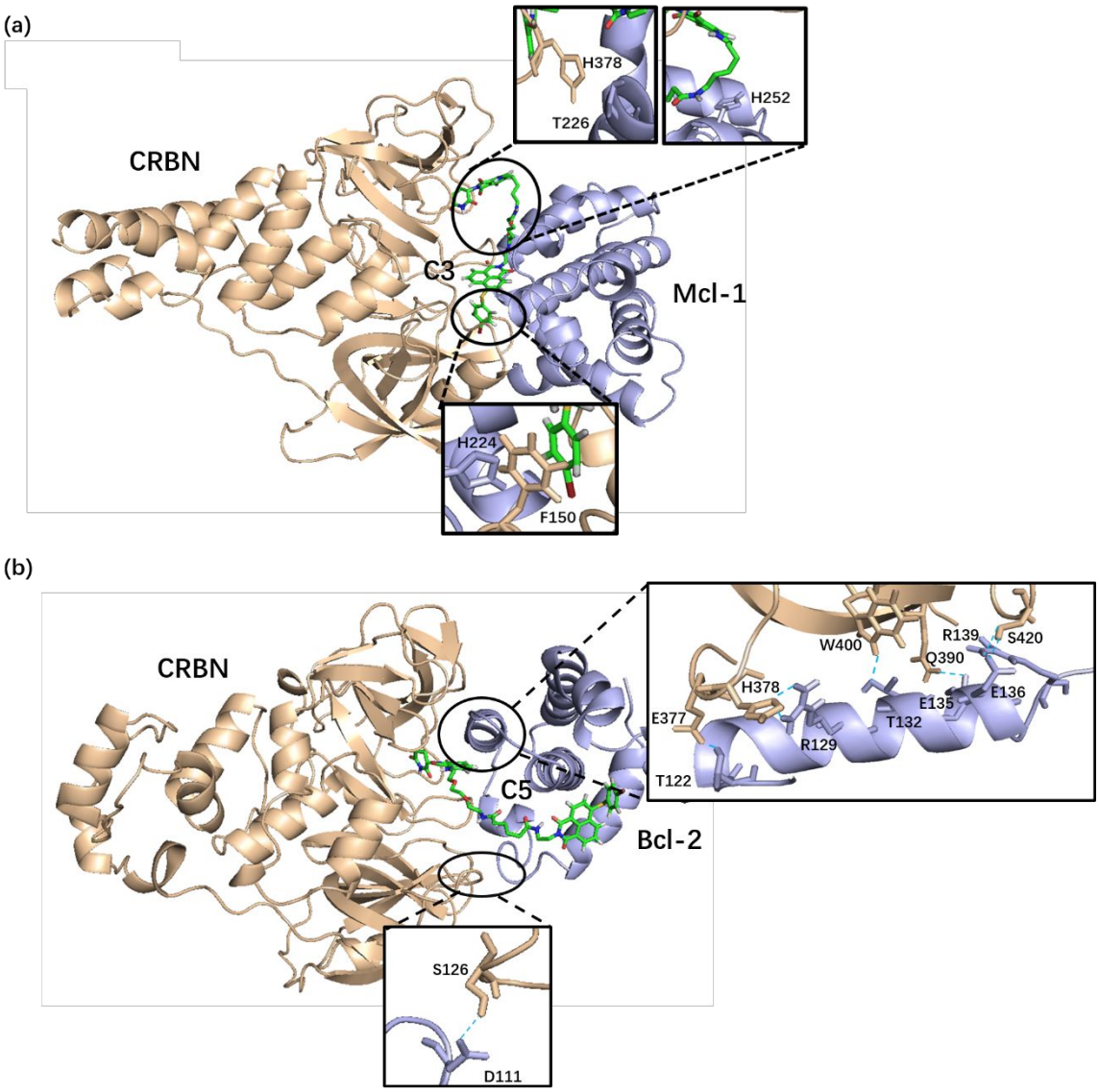

Figure 5. Favourable protein-protein interactions stabilize the **C3**/**C5**-induced complexes between Mcl-1/Bcl-2 and CRBN. (a) CRBN, **C3** and Mcl-1 and (b) CRBN, **C5** and Bcl-2

were docked and a 50-ns molecular dynamics simulation relaxed the structure (Mcl-1 PDB ID: 2PQK; Bcl-2 PDB ID: 2XA0; CRBN PDB ID:4TZ4)[42-44].

Next, we sought a molecular understanding of how Mcl-1 and Bcl-2 formed high-stability **C3**- and **C5**-induced ternary complexes with CRBN, respectively. To accomplish this, we docked previously published structures of Mcl-1/Bcl-2 and CRBN (PDB: 2PQK/2XA0 and 4TZ4)[42-44] with the **C3** and **C5** PROTACs, respectively, and applied 50-ns molecular dynamics simulations to relax each structure into a low energy conformation (Fig. 5 and Fig. S9).

According to the model shown in Fig. 5a, when the **C3** warhead engages Mcl-1, the **C3** alkyl linker region exhibits hydrophobic interactions with Histidine 252 in Mcl-1, and thus adopts a kinked conformation to accommodate the Mcl-1 α3 helix near CRBN. At the PPI interface between Mcl-1 and CRBN, Threonine 226 from Mcl-1 provides close, hydrophilic contacts to Histidine 378 in CRBN, and Histidine 224 from Mcl-1 creates an additional π-π stacking interaction with Phenylalanine 150 from CRBN. On the other hand, Bcl-2 forms a stable **C5**-induced ternary complex with CRBN (Fig. 4b). The **C5** PEG linker region adopts a linear conformation and points straight to the solvent, accommodating the Bcl-2 α4 helix near CRBN, indicating that the PPI interface is located on the Bcl-2 α4 helix. H-bonds are formed between Aspartic acid 111 from Bcl-2 and Serine 126 from CRBN; Glutamic acid 136 and Arginine 139 from Bcl-2 and Serine 420 from CRBN; Arginine 129 from Bcl-2 and Histidine 378 from CRBN; Threonine 122 from Bcl-2 and Glutamic acid 377 from CRBN; Threonine 132 from Bcl-2 and Tryptophan 400 from CRBN; and Glutamic acid 135 from Bcl-2 and Glutamine 390 from CRBN. In contrast, Mcl-1-**C5**-CRBN and Bcl-2-**C3**-CRBN showed no favourable energy conformation during 50-ns molecular dynamics simulations (Fig. S9).

Our MD illustrated the structure basis by which **C3** and **C5** induce ternary complexes between different target proteins and the E3 ligase, which offered a mechanism for the

above-mentioned inconsistency between binding affinity and degradation potency and selectivity. For example, the PROTAC-mediated protein-protein interfaces in the CRBN/Mcl-1 complex is not identical to those in CRBN/Bcl-2, illustrating the selectivity that **C3** and **C5** show for Mcl-1 and Bcl-2 degradation, respectively. Similarly, the lack of **C1**- and **C2**-induced degradation of Mcl-1 is likely due to steric clashes or hydrophobic collapse of their shorter hydrophobic linkers compared to **C3**. The longer linker in **C4** is also unfavorable for ternary complex formation. Meanwhile, PROTACs **H1-H5**, which connect to CRBN in an opposite orientation compared with **C1-C5**, showed almost no degradation activities, suggesting that conjugating the CRBN ligand near the Bcl-2 family protein P2 pocket can recruit the target proteins and E3 ligase into productive proximity.

As Bcl-2 family protein degradation can be potently observed with the PROTACs, we next sought to determine their cellular effects compared with the predominantly occupancy-based inhibitors. In a cell viability assay (Fig. 6a), we determined that the selective Mcl-1 degrader **C3** (DC_{50} = 0.76 μM) is much more active against the Mcl-1-driven H23 cell line than the parent inhibitor **Nap-1**, the N-methylated control compound **C3-Me** and the most powerful selective Mcl-1 inhibitor **A-1210477**[45] (IC_{50} = 0.03 μM, determined by cellular thermal shift assay, CETSA). The combination with **C3** and **C5** didn't show obvious synergistic effect (Fig. 6a), consistent with the fact that H23 is a Mcl-1-dependent cancer cell line. This results were further validated by PARP cleavage (Fig. 6b). Next, to evaluate whether the observed cytotoxic effects were truly driven by the efficiency of the PROTACs, we plotted the cytotoxicity % values from the cell viability assays relative to the Mcl-1 reduction % values (Fig. 6b) induced by **C3**. Strong correlation was observed between these two parameters (r^2 = 0.97, Fig. 6c), which is consistent with H23 cell proliferation being Mcl-1-driven. Overall, these results verified that PROTACs achieving *in cellulo* protein knockdown exhibited a better capacity to regulate cell phenotypic changes than the predominantly occupancy-based inhibitors.

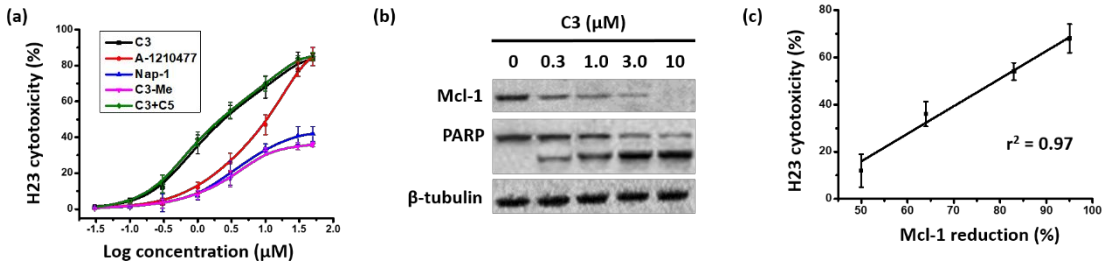

Figure 6. PROTACs exhibited better capacity to regulate cell phenotypic changes than the predominantly occupancy-based inhibitors. (a) Cell cytotoxicity assays in H23 cells upon addition of **C3**, **A-1210477**, **Nap-1**, **C3-Me** and a combination of **C3** with **C5** for 24 h. Percentages of cell viability were calculated by normalization of culture background without cells against untreated cultures as control. Data are expressed as the mean ± s.e.m. (n=3). (b) The levels of Mcl-1 and PARP cleavage were measured by western blot in H23 upon addition of a concentration gradient of **C3** for 12 h. All western blot figures represent the results from n = 3 independent samples. (c) Plotting the cytotoxicity % values in the H23 cells vs the Mcl-1 reduction % values induced by **C3**. Data are expressed as the mean ± s.e.m. (n=3).

Conclusion

In conclusion, we reported the first two PROTACs for PPI target degradation, which highlighted that PROTACs could expand the "target space" to PPI targets for which only weak binding ligands are available. These two PROTACs, **C3**/**C5**, produce potent, selective and reversible cellular Mcl-1/Bcl-2 knockdown and exhibit cytotoxicity driven by PROTAC efficiency, providing a new potent toolkit for selective chemical intervention of Bcl-2 family proteins in chemical biology research and drug discovery. Moreover, structure-activity relationship (SAR) analysis and MD simulations in a certain extent revealed the structural basis for turning nonselective or promiscuous target binding ligands into more selective degraders by changing the length and conformation of their linkers,

which is valuable for the design of other PROTACs.

Experimental Section.

Chemistry.

All commercial reagents were purchased and used without further purification or distillation unless otherwise stated. ^{1}H-NMR were obtained with a Bruker AV-500 or Bruker AV-400 spectrometer with chemical shifts reported as ppm (in DMSO, TMS as an internal standard). The following abbreviations are used for multiplicity of NMR signals: s=singlet, d=doublet, t=triplet. q=quartet, m=multiplet. High-resolution mass spectra (HRMS) were obtained on a MALDI-Tof MS (Micro) spectrometer. Column chromatography was performed on silica gel 200-300 mesh. The purity of all final products was determined by analytical HPLC-MS to be ≥ 95%.

Chemical synthesis of intermediate 1. (Scheme 1a)

To a suspension of 6-((4-bromophenyl)thio)-1-oxo-1H-phenalene-2,3-dicarbonitrile (417 mg, 1.0 mmol, 1.0 equiv) in a mixture of acetonitrile/H_2O (9:1, 20 mL) were added methyl 3-aminopropanoate hydrochloride (1.03 g, 10.0 mmol, 10.0 equiv) and NaOH (0.80 g, 20.0 mmol, 20.0 equiv). After stirring at rt for 1 h, the solvent was removed under reduced pressure and the crude was purified on silica gel (CH_2Cl_2/CH_3OH 30:1).

Methyl 3-((6-((4-bromophenyl)thio)-2-cyano-1-oxo-1H-phenalen-3-yl)amino)propanoate (1)

The expected product compound **1** was isolated as a yellow powder (133 mg, 27 %). ^{1}H NMR (400 MHz, $CDCl_3$): δ 8.59 (d, J=8.2 Hz, 2H), 8.46(d, J=8.3 Hz, 1H), 7.89 (t, J= 8.2 Hz, 1H), 7.64 (d, J=8.5 Hz, 2H), 7.57 (d, J=8.2 Hz,1H), 7.35 (d, J=8.5 Hz, 2H), 5.75 (s, 1H), 4.14 (q, J=6.9 Hz, 2H), 3.62 (s, 3H), 2.88 (t,J=6.9 Hz, 2H). TOF MS (ESI+): $C_{24}H_{17}N_2O_3SBr$, $[M+Na]^+$ calculated 517.01, 519.01, found 517.00, 519.03.

Chemical synthesis of intermediate 2. (Scheme 1b)

A mixture of 6-bromo-1H,3H-benzo[de]isochromene-1,3-dione(2.77 g, 10.0 mmol), 4-

bromobenzenethiol(2.08 g, 11.0 mmol) and triethylamine (1.5 mL) were stirred in DMF at 85 ºC for 6 h. The reaction mixture was first cooled to rt and then the pH was adjusted to 4 using 1 M HCl. The mixture was then filtered and the resulting solid was washed with water and ether and precipitated in petroleum ether/ethyl acetate (4:1), giving the desired product **5** (299 mg, 78.0 %) as a yellow solid. TOF MS (ESI+): $C_{18}H_9BrO_3S$, $[M+H]^+$ calculated 384.94, 386.94, found 384.97, 386.95.

In a round-bottom flask, a mixture of **5** (691 mg, 1.8 mmol), ethylenediamine (360 µL) and triethylamine (1.2 mL) were stirred in ethanol at 80 ºC for 6 h. The resulting mixture was concentrated under reduced pressure and the crude was purified on silica gel (CH_2Cl_2/MeOH 30:1). The expected product **6** was isolated as bring yellow flakes (500 mg, 68 %). TOF MS (EI+): $C_{20}H_{15}BrO_2N_2S$, $[M+H]^+$ calculated 427.00, 429.00, found 427.01, 429.01.

In a round-bottom flask, a mixture of **6** (300 mg, 0.702 mmol, 1.0 equiv), 6-Methoxy-6-oxohexanoic acid (124 mg, 0.772 mmol, 1.1 equiv), HATU (320 mg, 0.842 mmol, 1.2 equiv) were stirred in DCM (15 mL) and DIPEA (272 mg, 2.106 mmol, 3.0 equiv) was added at 0 ºC. The resulting mixture was stirred at rt overnight. The mixture was diluted with water (30 mL) and extracted with ethyl acetate (30 mL x 3). The combined organic layers were washed with brine (30 mL x 3), dried over anhydrous sodium sulfate, and evaporated under reduced pressure. The residue was purified on silica gel (CH_2Cl_2/MeOH 30:1).

Methyl-6-((2-(6-((4-bromophenyl)thio)-1,3-dioxo-1H-benzo[de]isoquinolin-2(3H)-yl)ethyl)amino)-6-oxohexanoate (2)

The expected product **2** was isolated as yellow flakes (200 mg, 50 %). ^{1}H NMR (500 MHz, $CDCl_3$): δ 8.65 (dd, J = 7.2, 6.2 Hz, 2H), 8.39 (d, J = 7.9 Hz, 1H), 7.82 – 7.78 (m, 1H), 7.59 – 7.55 (m, 2H), 7.39 – 7.35 (m, 2H), 7.34 (d, J = 7.9 Hz, 1H), 6.17 (s, 1H), 4.41 – 4.36 (m, 2H), 3.70 – 3.63 (m, 2H), 3.60 (s, 3H), 2.22 (dd, J = 8.7, 5.2 Hz, 2H), 2.11 (t, J = 7.0 Hz, 2H), 1.55 (dt, J = 7.2, 3.7 Hz, 4H). TOF MS (ESI+) $[C_{27}H_{26}BrN_2O_5S]^+$ calculated 569.06,

571.06, found 569.10, 571.09.

Chemical synthesis of CRBN binding intermediate 3 and 3-Me.

Compounds **3** and **3-Me** were facilely synthesized in high yield by the procedure as published in the literature.[40]

Chemical synthesis of intermediate C1-C6, C3-Me and C5-Me. (Scheme 1b)

General procedure.

Treatment of **2** (99 mg, 1 equiv, 1.0 mmol) with sodium hydroxide (80 mg, 2.00 mmol) gave compound **7** (88 mg, 92%) as orange flakes. ^{1}H NMR (400 MHz, $CDCl_3$): δ 12.19 (s, 1H), 8.58 (d, J=8.0 Hz, 2H), 8.46 (t, J=8.0 Hz, 2H), 7.88 (t, J= 8.0 Hz, 1H), 7.63 (d, J=8.5 Hz, 2H), 7.57 (d, J=8.1 Hz, 1H), 7.38 (d, J=8.5 Hz, 2H), 5.43 (s, 1H), 4.11 (q, J=6.9 Hz, 2H), 2.82 (t, J=6.9 Hz, 2H). TOF MS (ESI+): $C_{23}H_{15}N_2O_3SBr$, $[M+Na]^+$ calculated 577.08, found 577.10.

In a round-bottom flask, a mixture of **3/3-Me** (0.089 mmol 1.1 equiv), **7** (45 mg 0.081 mmol 1.0 equiv), HATU (37 mg 0.084 mmol 1.2 equiv) were stirred in DCM (15 mL) and DIPEA (31 mg 0.24 mmol 3.0 equiv) was added at 0 ºC. The resulting mixture was stirred at rt overnight. The mixture was diluted with water (30mL) and extracted with ethyl acetate (30 mL × 3). The combined organic layers were washed with brine (30 mL × 3), dried over anhydrous sodium sulfate, and evaporated under reduced pressure. The residue was purified on silica gel (CH_2Cl_2/MeOH 30:1). The expected product **C1-C6/C3-Me/C5-Me** was isolated as yellow flakes.

N1-(2-(6-((4-bromophenyl)thio)-1,3-dioxo-1H-benzo[de]isoquinolin-2(3H)-yl)ethyl)-N6-(2-((2-(2,6-dioxopiperidin-3-yl)-1,3-dioxoisoindolin-4-yl)amino)ethyl)adipamide (C1).

41 mg, yield = 60 %. ^{1}H NMR (500 MHz, $CDCl_3$) δ 8.65 – 8.61 (m, 2H), 8.41 (s, 1H), 8.37 (d, J = 7.9 Hz, 1H), 7.81 – 7.77 (m, 1H), 7.60 – 7.55 (m, 2H), 7.49 – 7.44 (m, 1H), 7.39 – 7.36 (m, 2H), 7.31 (d, J = 7.9 Hz, 1H), 7.06 (d, J = 7.1 Hz, 1H), 6.87 (d, J = 8.5 Hz, 1H), 6.32 (s, 1H), 6.19 (t, J = 5.6 Hz, 1H), 6.12 (t, J = 5.6 Hz, 1H), 4.91 (dd, J = 12.2, 5.4

Hz, 1H), 4.36 (t, J = 5.6 Hz, 2H), 3.71 (m, J = 13.8, 6.8 Hz, 2H), 3.40 – 3.11 (m, 4H), 2.20 – 2.04 (m, 8H), 1.58 – 1.37 (m, 4H). [TOF MS (ESI+)]: $C_{41}H_{37}BrN_6O_8S$ [M+Na^+], calculated 875.146917, found 875.14677

N1-(2-(6-((4-bromophenyl)thio)-1,3-dioxo-1H-benzo[de]isoquinolin-2(3H)-yl)ethyl)-N6-(4-((2-(2,6-dioxopiperidin-3-yl)-1,3-dioxoisoindolin-4-yl)amino)butyl)adipamide (C2).

49 mg, yield = 62 %. ^{1}H NMR (500 MHz, $CDCl_3$) δ 8.80 (s, 1H), 8.61 (t, J = 7.8 Hz, 2H), 8.35 (d, J = 7.9 Hz, 1H), 7.83 – 7.72 (m, 1H), 7.57 (d, J = 8.5 Hz, 2H), 7.50 – 7.42 (m, 1H), 7.37 (d, J = 8.4 Hz, 2H), 7.27 (d, J = 7.5 Hz, 1H), 7.07 (d, J = 7.1 Hz, 1H), 6.92 (d, J = 8.5 Hz, 1H), 6.64 (s, 1H), 6.48 – 6.36 (m, 2H), 4.91 (dd, J = 12.2, 5.4 Hz, 1H), 4.32 (dd, J = 12.5, 7.4 Hz, 2H), 3.61 (tt, J = 14.3, 7.2 Hz, 2H), 2.80 – 2.69 (m, 4H), 2.17 – 2.01 (m, 8H), 1.53 – 1.36 (m, 8H). [TOF MS (ESI+)]: $C_{43}H_{41}BrN_6O_8S$ [M+Na^+], calculated 903.178217, found 903.17781

N1-(2-(6-((4-bromophenyl)thio)-1,3-dioxo-1H-benzo[de]isoquinolin-2(3H)-yl)ethyl)-N6-(7-((2-(2,6-dioxopiperidin-3-yl)-1,3-dioxoisoindolin-4-yl)amino)heptyl)adipamide (C3).

64mg, yield = 56 %. ^{1}H NMR (400 MHz, $CDCl_3$) δ 8.64 (dd, J = 7.9, 3.8 Hz, 2H), 8.38 (d, J = 7.9 Hz, 1H), 8.26 (s, 1H), 7.85 – 7.76 (m, 1H), 7.60 – 7.56 (m, 2H), 7.50 – 7.45 (m, 1H), 7.40 – 7.36 (m, 2H), 7.32 (d, J = 7.9 Hz, 1H), 7.08 (d, J = 7.1 Hz, 1H), 6.86 (d, J = 8.5 Hz, 1H), 6.22 (d, J = 6.2 Hz, 2H), 5.83 (s, 1H), 4.91 (dd, J = 12.1, 5.4 Hz, 1H), 4.41 – 4.34 (m, 2H), 3.66 (m, 2H), 3.25 (dd, J = 12.6, 6.6 Hz, 2H), 3.16 (dd, J = 12.9, 6.9 Hz, 2H), 2.15 – 2.03 (m, 8H), 1.65 (m, 6H), 1.51 – 1.45 (m, 4H), 1.44 (d, J = 6.8 Hz, 2H). [TOF MS (ESI+)]: $C_{45}H_{45}BrN_6O_8S$ [M+Na^+], calculated 931.209517, found 931.21017.

N^1-(2-(6-((4-bromophenyl)thio)-1,3-dioxo-1H-benzo[de]isoquinolin-2(3H)-yl)ethyl)-N^6-(6-((2-(1-methyl-2,6-dioxopiperidin-3-yl)-1,3-dioxoisoindolin-4-yl)amino)hexyl)adipamide (C3-Me).

45 mg, yield = 60 %. ^{1}H NMR (400 MHz, $CDCl_3$) δ 8.66 (dd, J = 7.8, 3.8 Hz, 2H), 8.38

(d, J = 7.8 Hz, 1H), 8.26 (s, 1H), 7.85 – 7.76 (m, 1H), 7.61 – 7.56 (m, 2H), 7.50 – 7.45 (m, 1H), 7.40 – 7.36 (m, 2H), 7.32 (d, J = 7.9 Hz, 1H), 7.11 (d, J = 7.0 Hz, 1H), 6.89 (d, J = 8.5 Hz, 1H), 6.23 (d, J = 6.2 Hz, 2H), 5.85 (s, 1H), 4.91 (dd, J = 12.1, 5.4 Hz, 1H), 4.41 – 4.34 (m, 2H), 3.66 (m, 2H), 3.25 (dd, J = 12.6, 6.6 Hz, 2H), 3.21 (s, 3H), 3.16 (dd, J = 12.9, 6.9 Hz, 2H), 2.15 – 2.03 (m, 8H), 1.65 (m, 6H), 1.51 – 1.45 (m, 4H), 1.44 (d, J = 6.8 Hz, 2H). [TOF MS (ESI+)]: $C_{46}H_{47}BrN_6O_8S$ [M+Na^+], calculated 945.2252, found 945.2258.

N1-(2-(6-((4-bromophenyl)thio)-1,3-dioxo-1H-benzo[de]isoquinolin-2(3H)-yl)ethyl)-N6-(6-((6-((2-(2,6-dioxopiperidin-3-yl)-1,3-dioxoisoindolin-4-yl)amino)hexyl)amino)-6-oxohexyl)adipamide (C4).

69 mg, yield = 50 %. ^{1}H NMR (500 MHz, $CDCl_3$) δ 8.64 (dd, J = 7.9, 3.0 Hz, 2H), 8.49 (s, 1H), 8.37 (d, J = 7.9 Hz, 1H), 7.80 (dd, J = 8.4, 7.4 Hz, 1H), 7.59 – 7.57 (m, 2H), 7.48 (dd, J = 8.4, 7.2 Hz, 1H), 7.40 – 7.36 (m, 2H), 7.31 (d, J = 7.9 Hz, 1H), 7.07 (d, J = 7.0 Hz, 1H), 6.87 (d, J = 8.6 Hz, 1H), 6.33 (s, 1H), 6.21 (s, 1H), 5.92 (s, 1H), 5.88 (s, 1H), 4.92 (dd, J = 12.3, 5.4 Hz, 1H), 4.40 – 4.34 (m, 2H), 3.70 – 3.60 (m, 2H), 3.23 (m, 4H), 3.14 (m, 2H), 2.82 – 2.68 (m, 2H), 2.16 – 2.08 (m, 8H), 2.06 (d, J = 6.6 Hz, 2H), 1.55 – 1.47 (m, 8H), 1.43 (m, 8H). [TOF MS (ESI+)]: $C_{51}H_{56}BrN_7O_9S$ [M+Na^+], calculated 1044.293581, found 1044.29318

N1-(2-(6-((4-bromophenyl)thio)-1,3-dioxo-1H-benzo[de]isoquinolin-2(3H)-yl)ethyl)-N6-(2-(2-(2-((2-(2,6-dioxopiperidin-3-yl)-1,3-dioxoisoindolin-4-yl)amino)ethoxy)ethoxy)ethyl)adipamide (C5).

35 mg, yield = 52 %. ^{1}H NMR (400 MHz, $CDCl_3$) δ 9.24 (s, 1H), 8.62 (dd, J = 10.3, 7.9 Hz, 2H), 8.37 (d, J = 7.9 Hz, 1H), 7.79 (dd, J = 8.3, 7.5 Hz, 1H), 7.61 – 7.54 (m, 2H), 7.51 – 7.45 (m, 1H), 7.40 – 7.35 (m, 2H), 7.31 (d, J = 7.9 Hz, 1H), 7.09 (d, J = 7.1 Hz, 1H), 6.88 (d, J = 8.5 Hz, 1H), 6.53 (t, J = 5.3 Hz, 1H), 6.41 (t, J = 5.1 Hz, 1H), 6.29 (t, J = 5.2 Hz, 1H), 4.96 – 4.87 (m, 1H), 4.39 – 4.30 (m, 2H), 3.72 (t, J = 5.1 Hz, 2H), 3.66 – 3.61 (m, 6H), 3.55 (t, J = 5.0 Hz, 2H), 3.45 (dd, J = 10.4, 5.2 Hz, 2H), 3.39 (dd, J = 10.5, 5.3 Hz, 2H), 2.07 (dt, J = 6.7, 3.4 Hz, 8H), 1.54 – 1.49 (m, 4H). [TOF MS (ESI+)]: $C_{45}H_{45}BrN_6O_{10}S$

[M+Na$^+$], calculated 963.199346, found 963.19903.

N^1-(2-(6-((4-bromophenyl)thio)-1,3-dioxo-1H-benzo[de]isoquinolin-2(3H)-yl)ethyl)-N^6-(2-(2-(2-((2-(1-methyl-2,6-dioxopiperidin-3-yl)-1,3-dioxoisoindolin-4-yl)amino)ethoxy)ethoxy)ethyl)adipamide (C5-Me).

43 mg, yield = 55 %. ^{1}H NMR (400 MHz, $CDCl_3$) δ 9.26 (s, 1H), 8.60 (dd, J = 10.3, 7.9 Hz, 2H), 8.39 (d, J = 7.9 Hz, 1H), 7.81 (dd, J = 8.3, 7.5 Hz, 1H), 7.60 – 7.54 (m, 2H), 7.52 – 7.44 (m, 1H), 7.40 – 7.35 (m, 2H), 7.31 (d, J = 7.9 Hz, 1H), 7.09 (d, J = 7.1 Hz, 1H), 6.88 (d, J = 8.5 Hz, 1H), 6.53 (t, J = 5.3 Hz, 1H), 6.41 (t, J = 5.1 Hz, 1H), 6.29 (t, J = 5.2 Hz, 1H), 4.97 – 4.89 (m, 1H), 4.39 – 4.31 (m, 2H), 3.73 (t, J = 5.1 Hz, 2H), 3.66 – 3.61 (m, 6H), 3.57 (t, J = 5.0 Hz, 2H), 3.46 (dd, J = 10.4, 5.2 Hz, 2H), 3.41 (dd, J = 10.5, 5.3 Hz, 2H), 3.21 (s, 3H), 2.08 (dt, J = 6.7, 3.4 Hz, 8H), 1.54 – 1.48 (m, 4H). [TOF MS (ESI+)]: $C_{46}H_{47}BrN_6O_{10}S$ [M+Na$^+$], calculated 977.2150, found 977.2154.

N^1-(2-(6-((4-bromophenyl)thio)-1,3-dioxo-1H-benzo[de]isoquinolin-2(3H)-yl)ethyl)-N^6-(8-((2-(2,6-dioxopiperidin-3-yl)-1,3-dioxoisoindolin-4-yl)amino)octyl)adipamide (C6).

44mg, yield = 59 %. ^{1}H NMR (400 MHz, $CDCl_3$) δ 8.64 (dd, J = 7.9, 3.8 Hz, 2H), 8.38 (d, J = 7.9 Hz, 1H), 8.26 (s, 1H), 7.85 – 7.76 (m, 1H), 7.60 – 7.56 (m, 2H), 7.50 – 7.45 (m, 1H), 7.40 – 7.36 (m, 2H), 7.33 (d, J = 7.9 Hz, 1H), 7.10 (d, J = 7.1 Hz, 1H), 6.86 (d, J = 8.5 Hz, 1H), 6.22 (d, J = 6.2 Hz, 2H), 5.83 (s, 1H), 4.91 (dd, J = 12.1, 5.4 Hz, 1H), 4.41 – 4.34 (m, 2H), 3.66 (m, 2H), 3.25 (dd, J = 12.6, 6.6 Hz, 2H), 3.16 (dd, J = 12.9, 6.9 Hz, 2H), 2.15 – 2.03 (m, 8H), 1.63 (m, 6H), 1.54 – 1.45 (m, 8H), 1.44 (d, J = 6.8 Hz, 2H). [TOF MS (ESI+)]: $C_{47}H_{49}BrN_6O_8S$ [M+H$^+$], calculated 937.2589, found 937.2581.

Chemical synthesis of intermediate H1-H5. **(Scheme 1a)**

General procedure.

Treatment of **1** (99 mg, 1 equiv, 1.0 mmol) with sodium hydroxide (80 mg, 2.00 mmol) gave compound **S1-5** (88 mg, 92%) as orange flakes. ^{1}H NMR (400 MHz, $CDCl_3$): δ 12.19 (s, 1H), 8.58 (d, J=8.0 Hz, 2H), 8.46 (t, J=8.0 Hz, 2H), 7.88 (t, J= 8.0 Hz, 1H), 7.63 (d,

J=8.5 Hz, 2H), 7.57 (d, J=8.1 Hz, 1H), 7.38 (d, J=8.5 Hz, 2H), 5.43 (s, 1H), 4.11 (q, J=6.9 Hz, 2H), 2.82 (t, J=6.9 Hz, 2H). TOF MS (ESI+): $C_{23}H_{15}N_2O_3SBr$, $[M+Na]^+$ calculated 502.9864, found 502.9870.

In a round-bottom flask, a mixture of **3** (0.092 mmol, 1.1 equiv), **S1-5** (40 mg, 0.084 mmol, 1.0 equiv), HATU (38 mg, 0.1 mmol, 1.2 equiv) were stirred in DCM (15 mL) and DIPEA (32 mg, 0.25 mmol, 3.0 equiv) was added at 0 ºC. The resulting mixture was stirred at rt overnight. The mixture was diluted with water (30 mL) and extracted with ethyl acetate (30 mL x 3). The combined organic layers were washed with brine (30 mL x 3), dried over anhydrous sodium sulfate, and evaporated under reduced pressure. The residue was purified on silica gel (CH_2Cl_2/MeOH 30:1). The expected product **H1-H5** was isolated as orange flakes.

3-((6-((4-bromophenyl)thio)-2-cyano-1-oxo-1H-phenalen-3-yl)amino)-N-(2-((2-(2,6-dioxopiperidin-3-yl)-1,3-dioxoisoindolin-4-yl)amino)ethyl)propanamide (H1).

39 mg, yield = 61 %. ^{1}H NMR (500 MHz, DMSO) δ 11.08 (s, 1H), 8.71 (s, 1H), 8.57 (d, J = 8.4 Hz, 1H), 8.45 (d, J = 7.2 Hz, 1H), 8.40 (d, J = 8.1 Hz, 1H), 8.29 (s, 1H), 7.90 – 7.84 (m, 1H), 7.63 (d, J = 8.5 Hz, 2H), 7.50 (t, J = 7.3 Hz, 2H), 7.38 (d, J = 8.4 Hz, 2H), 7.07 (d, J = 8.6 Hz, 1H), 6.97 (d, J = 7.1 Hz, 1H), 6.69 (s, 1H), 5.01 (dd, J = 12.8, 5.5 Hz, 1H), 4.13 (d, J = 6.1 Hz, 2H), 3.25 (m, 4H), 2.64 (t, J = 6.5 Hz, 2H), 2.02 – 1.93 (m, 4H). [TOF MS (ESI+)]: $C_{38}H_{29}BrN_6O_6S$ $[M+Na^+]$ calculated 799.094487, found 799.09364

3-((6-((4-bromophenyl)thio)-2-cyano-1-oxo-1H-phenalen-3-yl)amino)-N-(4-((2-(2,6-dioxopiperidin-3-yl)-1,3-dioxoisoindolin-4-yl)amino)butyl)propanamide (H2)

35 mg, yield = 52%. ^{1}H NMR (400 MHz, $CDCl_3$) δ 8.77 (s, 1H), 8.51 – 8.38 (m, 3H), 7.91 (d, J = 8.2 Hz, 1H), 7.66 (t, J = 7.8 Hz, 1H), 7.56 (d, J = 8.4 Hz, 2H), 7.36 (d, J = 8.4 Hz, 2H), 7.33 – 7.28 (m, 1H), 7.14 (d, J = 8.1 Hz, 1H), 7.06 (s, 1H), 6.92 (d, J = 7.1 Hz, 1H), 6.70 (d, J = 8.5 Hz, 1H), 6.12 (d, J = 5.3 Hz, 1H), 4.89 (dd, J = 12.1, 5.5 Hz, 1H), 4.28 (s, 2H), 3.33 (d, J = 5.3 Hz, 2H), 3.19 (d, J = 5.4 Hz, 2H), 2.88 – 2.66 (m, 4H), 1.51 – 1.47 (m, 4H), 1.43 (d, J = 6.0 Hz, 2H). [TOF MS (ESI+)]: $C_{40}H_{33}BrN_6O_6S$ $[M+Na^+]$, calculated

827.125788, found 827.12489

3-((6-((4-bromophenyl)thio)-2-cyano-1-oxo-1H-phenalen-3-yl)amino)-N-(6-((2-(2,6-dioxopiperidin-3-yl)-1,3-dioxoisoindolin-4-yl)amino)hexyl)propanamide (H3)

52 mg, yield = 56%. ^{1}H NMR (500 MHz, $CDCl_3$) δ 8.58 (d, J = 7.2 Hz, 1H), 8.52 (d, J = 8.4 Hz, 1H), 8.41 (s, 1H), 8.33 (s, 1H), 7.91 (d, J = 8.3 Hz, 1H), 7.72 (t, J = 7.8 Hz, 1H), 7.56 (d, J = 8.3 Hz, 2H), 7.40 (t, J = 7.9 Hz, 1H), 7.36 (d, J = 8.3 Hz, 2H), 7.20 (d, J = 8.1 Hz, 1H), 6.99 (d, J = 7.1 Hz, 1H), 6.79 (d, J = 8.6 Hz, 1H), 6.43 (s, 1H), 6.16 (s, 1H), 4.90 (dd, J = 11.9, 5.4 Hz, 1H), 4.30 (d, J = 4.6 Hz, 2H), 3.29 (d, J = 6.1 Hz, 2H), 3.21 (dd, J = 12.3, 6.4 Hz, 2H), 2.74 (dd, J = 15.3, 4.2 Hz, 2H), 2.01 – 1.91 (m, 4H), 1.65 – 1.54 (m, 2H), 1.36 – 1.17 (m, 6H). [TOF MS (ESI+)]: $C_{42}H_{37}BrN_6O_6S$, found 855.1579, 857.1554

6-(3-((6-((4-bromophenyl)thio)-2-cyano-1-oxo-1H-phenalen-3-yl)amino)propanamido)-N-(6-((2-(2,6-dioxopiperidin-3-yl)-1,3-dioxoisoindolin-4-yl)amino)hexyl)hexanamide (H4)

42 mg, yield = 45%. ^{1}H NMR (400 MHz, $CDCl_3$) δ 8.71 (s, 1H), 8.57 (t, J = 6.9 Hz, 2H), 8.27 (s, 1H), 8.00 (d, J = 8.3 Hz, 1H), 7.78 – 7.73 (m, 1H), 7.59 – 7.55 (m, 2H), 7.49 – 7.41 (m, 1H), 7.38 – 7.33 (m, 2H), 7.22 (d, J = 8.2 Hz, 1H), 7.04 (d, J = 6.9 Hz, 1H), 6.84 (d, J = 8.5 Hz, 1H), 6.75 (s, 1H), 6.19 (s, 1H), 5.79 (s, 1H), 4.93 – 4.88 (m, 1H), 4.28 (m, 2H), 3.29 – 3.14 (m, 8H), 2.74 – 2.68 (m, 2H), 2.25 – 2.11 (m, 4H), 1.53 – 1.39 (m, 14H). [TOF MS (ESI+)]: $C_{48}H_{48}BrN_7O_7S$ [M+Na^+], calculated 968.241152, found 968.24052

3-((6-((4-bromophenyl)thio)-2-cyano-1-oxo-1H-phenalen-3-yl)amino)-N-(2-(2-(2-((2-(2,6-dioxopiperidin-3-yl)-1,3-dioxoisoindolin-4-yl)amino)ethoxy)ethoxy)ethyl)propanamide (H5)

38mg, yield = 53%. ^{1}H NMR (400 MHz, $CDCl_3$) δ 9.13 (s, 1H), 8.56 (d, J = 7.3 Hz, 1H), 8.49 (d, J = 8.4 Hz, 1H), 8.23 (s, 1H), 7.91 (d, J = 8.2 Hz, 1H), 7.70 (t, J = 7.8 Hz, 1H), 7.56 (d, J = 8.4 Hz, 2H), 7.37 (d, J = 8.4 Hz, 2H), 7.32 – 7.27 (m, 1H), 7.16 (dd, J = 8.1, 3.8 Hz, 1H), 7.10 (s, 1H), 6.88 (d, J = 7.0 Hz, 1H), 6.78 (d, J = 8.5 Hz, 1H), 6.50 (s, 1H), 4.90 (dd, J = 11.9, 5.7 Hz, 1H), 4.27 (m, 2H), 3.67 (m, 4H), 3.64 – 3.59 (m, 4H), 3.50 –

3.41 (m, 6H), 2.18 – 1.93 (m, 4H). [TOF MS (ESI+)]: $C_{42}H_{37}BrN_6O_8S$ [M+Na^+], calculated 887.146917, found 887.1732

Protein Expression and Purification.

The plasmid expressing Mcl-1 and Bcl-2 wconstructed as described in our previous study.[36] The two proteins with an N-terminal 8 × His tag was produced in Escherichia coli BL21 (DE3) cells. Cells were grown at 37 °C in LB containing 30 μg/mL Kana. Protein expression was induced by 0.4 mM IPTG at 37 °C for 4h. Cells were lysed in PBS containing 1 mM PMSF. The protein was purified from the soluble fraction using Ni-NTA resin (Qiagen, Hilden, Germany), following the manufacturer's instructions. The protein was further purified on a Source Q15 column in 25 mM Tris pH 8.0 buffer, with a NaCl gradient.

Enzyme-linked immunosorbent assay (ELISA)

R-(-)-Gossypol was used as a positive control. For this assay, biotinylated Bim peptide (residues 81–106, biotin-(β)A-(β)A-D-M-R-P-E-I-W-I-A-Q-E-L-R-R-I-G-D-E-F-N-A-Y-Y-A-R-R-amide, hereafter called biotin-Bim) was diluted to 0.09 mg/mL in SuperBlock blocking buffer in PBS (Pierce Biotechnology, Inc, Rockford, IL, catalog #37515) and incubated for 1.5 h in 96-well microtiter plates already coated with streptavidin (Qiagen, catalog #15500) to allow the formation of the complex between Biotin-Bim and streptavidin. All incubations were performed at 4 ℃ unless otherwise noted. Each inhibitor was first dissolved in pure DMSO to obtain a 10 mM stock solution. Then the stock solution was diluted successively to get the solution with different concentration gradients (100 μM, 50 μM, 10 μM, 5 μM, 3 μM, 1 μM, 0.5 μM, 0.1 μM). For each tested inhibitor, different concentrations of the inhibitor were incubated with 200 nM His-tagged Mcl-1 or Bcl-2 protein in PBS for 1 h with a final DMSO concentration of 4%. The plates were washed three times with PBS containing 0.05% Tween-20. The inhibitor and protein mixture (100 mL) were transferred to the plate containing the biotin-Bim/streptavidin complex and incubated for 2 h. The plate was then washed as before and mouse anti-His antibody that

was conjugated with horseradish peroxidase (Qiagen, catalog #34460) was added into the wells and incubated for 1 h. The plate was then washed with PBS containing 0.05% Tween-20. Finally, TMB (100 mL, Beyotime, catalog #P0209) was added to each well; the enzymatic reaction was stopped after 30 min by addition of H_2SO_4 (100 mL, 2 M). Absorbances were measured with a TECAN GENios (Swiss, TECAN) microplate reader using a wavelength of 450 nm. Three independent experiments were performed with each inhibitor to calculate average IC_{50} value and standard deviation (SD). (-)-Gossypol was used as comparison in our assay.

Cell Culture

The human cervical carcinoma cells (Hela) was obtained from the Typical Culture Preservation Commission Cell Bank (Chinese Acadamy of Sciences, Shanghai, China) and maintained in DMEM/HIGH GLUCOSE (Hyclone, Beijing, China) supplemented with 10% fetal bovine serum (Gibco Company, USA). The human chronic myelogenous leukemia cells (K562) and human lung cells (NCI-H23) were obtained from the Typical Culture Preservation Commission Cell Bank and maintained in RPMI1640 (Hyclone, Beijing, China) media supplemented with 10% fetal bovine serum. All cells were cultured at 37°C in 5% CO_2.

Immunoblotting.

Cells were lysed in NP-40 lysis buffer (0.2% NP-40, 142.5 mM KCl, 5 mM $MgCl_2$, 1 mM EGTA, and 20 mM HEPES at pH 7.5) containing 1 mM PMSF, 1 μg/mL aprotinin, 1 μg/mL leupeptin, and 1 μg/mL pepstatin. Protein concentrations were determined by BCA assay (Pierce Chemical, IL, USA). Equal protein concentrations of each sample were subjected to sodium dodecyl sulfate polyacrylamide gel electrophoresis (SDS-PAGE) and electrophoretically transferred to polyvinylidene difluoride membranes. Membranes were blocked with TBS containing 5% skim milk and 0.1% Tween 20 and then probed with specific antibodies. Blots were developed using enhanced chemiluminescence kit (Amersham Biosciences, San Diego, CA, USA) according to the manufacturer's

instructions. All immunonloting experiments were repeated with n = 3 independent samples.

The ternary complexes detecting assay.

Hela (25×10^6) were lysed in 1% Triton X-100 IP buffer (Beyotime, Shanghai, China). Whole-cell lysates were obtained, 1 mg total proteins were incubated overnight with 1 μg of the specific CRBN-antibody. The ternary complexes were captured with protein A+G Agarose (Santa Cruz Biotechnology, CA, USA), washed three times with Triton X-100 buffer and boiled in loading buffer (Invitrogen, Carlsbad, CA, USA). The constitutes of the ternary complexes was performed by immunoblotting using specific Mcl-1, Bcl-2 and CRBN antibodies as described above.[8,9] This assay was repeated with n = 3 independent samples.

Molecular docking

The 3D structure of Mcl-1 (PDB ID: 2PQK) was obtained from the protein bank in the RCSB. The mol2 structures of the inhibitors were generated using Chembio3D Ultra 11.0 followed by energy minimization. AutoDock 4.2 program equipped with ADT was used to perform the automated molecular docking. Grid maps covering residues that were perturbed more than the threshold value of 0.1 ppm in the binding groove of the proteins were defined for all inhibitors in the AutoDock calculations using a grid spacing about of 0.375 Å. For each docking job, 100 hybrid GALS runs were carried-out. A total of 100 possible binding conformations were generated and grouped into clusters based on a 1.0 Å cluster tolerance. The docking models were analyzed and represented using ADT.

Molecular Dynamics (MD) Simulations

The starting structures for CRBN came from the crystal structure downloaded from Protein Data Bank (PDB) entry 4TZ4. In order to replace the ligand in this structure with pomalidomide, the PDB entry 4TZU was used by aligning its protein backbone to that of 4TZ4, transferring pomalidomide to the 4TZ4 structure and replacing the original ligand. The starting structures for Mcl-1 or Bcl-2 (PDB: 2PQK or 2XA0) and **2** complexes was

the best pose obtained from the docking study. The starting structures for the Mcl-1 (or Bcl-2): PROTAC: Cereblon trimer were prepared in a way that the hydrophobic patch of CRBN-ligand surface opposed different hydrophobic patches and grooves of the Mcl-1-ligand surface, thus producing different starting modes in terms of the relative dispositions between CRBN and Mcl-1. For each starting mode, a linker was built to connect pomalidomide and Mcl-1 ligand and form the full PROTAC. And an energy minimization was performed for each starting point of trimer. All the molecular-dynamics (MD) simulations were performed in Gromacs 4.6.7 with GROMOS 96 43A1 force-field for proteins and ligands were prepared using PRODRG 2.5 server. The protocol of the MD simulation was as follows: The complex structure was solvated in a truncated dodecahedron SPC water box 10 Å from the edge and the positive charge of the system was neutralized by adding Cl^- counter ions. The system was energy minimized with the steepest descent algorithm for 1000 steps. Thereafter, 1 ns isothermal-isochoric (NVT, with T = 300 K) and 1 ns isothermal-isobaric (NPT, with T = 300 K and P =1 atm) MD simulations were performed to equilibrate the system. The harmonic restraint with a force constant of 1000 kJ mol^{-1} nm^{-2} was used during the simulations. The equilibrated system was then subjected to a simulation of 50 ns without any restraint. Two independent MD runs were performed for each complex for ensemble convergence. During the equilibration and production runs, the time step was 2 fs, and the LINCS algorithm was applied to constrain the bonds involving hydrogens. The van der Waals and short-range electrostatic interactions cutoff was set to 14 Å, and the particle-mesh Ewald (PME) method was used to treat long-range electrostatics.

Cell Viability Assays

H23 cells were incubated with compounds at the desired concentration for 24 h on a clear-bottom 96-well plate. Cells were kept in RPMI medium supplemented with 10 % FBS, L-glutamine, penicillin, and streptomycin. Initial cell density was 4×10^4 per mL. Cells were treated with various concentrations of compound or vehicle DMSO (0.05 %).

After treatment, cell viability was measured with cell counting kit 8 (CCK8) cell viability assay kit according to the manufacturer instructions. Percentages of cell viability were calculated by normalization of culture background without cells against untreated cultures as control.

Supporting Information:

Binding affinity curves to Mcl-1/Bcl-2; Time/dose-dependent western blots and quantification of protein levels in Hela and K562 cells; mRNA levels during PROTACs treatment in Hela cells; Protein levels of Bcl-xl, MDM2 and tubulin during PROTACs treatment in Hela cells; Co-IP of Mcl-1/Bcl-2 and CRBN upon **H3** treatment; NMR and LC-MS spectra of key compounds (PDF)

Molecular formula strings (CSV)

The MD-simulated structure of ternary complexes Mcl1-**C3**-CRBN and Bcl2-**C5**-CRBN (PDB)

Corresponding Author Information:

*Phone: +86 411 84986032. Fax: +86 411 84986032. E-mail: zczhang@dlut.edu.cn.

Acknowledgment: This research was supported by the National Natural Science Foundation of China (81570129, 21502015, and 81430083) and the China Postdoctoral Science Foundation (2018M641694).

Abbreviations

SAR, structure-activity relationship; PPI, protein-protein interaction; PROTACs, Proteolysis Targeting Chimeras; BET, bromodomains and extra-terminal; MD, molecular dynamics; CRBN, cereblon; DMSO, dimethyl sulfoxide; DMF, N,N-dimethylformamide; DCM, dimethyl chloride; THF, tetrahydrofuran; DIEA, N,N-di-isopropylethylamine; HATU, hexafluorophosphate azabenzotriazole tetramethyl uranium.

Reference:

1. A. C. Lai and C. M. Crews. Induced protein degradation: an emerging drug discovery paradigm. *Nat. Rev. Drug Discov.* **2017**, *16*, 101-114.
2. M. Toure and C. M. Crews. Small-molecule PROTACS: new approaches to protein degradation. *Angew. Chem. Int. Ed.* **2016**, *55*, 1966-1973.
3. P. M. Cromm and C. M. Crews. Targeted protein degradation: from chemical biology to drug discovery. *Cell Chem. Biol.* **2017**, *24*, 1181-1190.
4. I. Churcher. Protac-induced protein degradation in drug discovery: breaking the rules or just making new ones? *J. Med. Chem.* **2018**, *61*, 444-452.
5. L. Tan and N. S. Gray. When kinases meet PROTACs. *Chin. J. Chem*. **2018**, *36*, 971-977.
6. X. Lucas and A. Ciulli. Recognition of substrate degrons by E3 ubiquitin ligases and modulation by small-molecule mimicry strategies. *Curr. Opin. Struct. Biol*. **2017**, *44*, 101-110.
7. V. Zoppi, S. J. Hughes, C. Maniaci, A. Testa, T. Gmaschitz, C. Wieshofer, M. Koegl, M. K. Riching, L. D. Daniels, A. Spallarossa, and A.Ciulli. Iterative design and optimization of initially inactive proteolysis targeting chimeras (PROTACs) identify VZ185 as a potent, fast, and selective von hippel-lindau (VHL) based dual degrader probe of BRD9 and BRD7. *J. Med. Chem.* **2018**, *62*, 699-726.
8. D. P. Bondeson, A. Mares, I. E. Smith, E. Ko, S. Campos, A. H. Miah, K. E. Mulholland, N. Routly, D. L. Buckley, J. L. Gustafson, N. Zinn, P. Grandi, S. Shimamura, G. Bergamini, M. Faelth-Savitski, M. Bantscheff, C. Cox, D. A. Gordon, R. R. Willard, J. J. Flanagan, L. N. Casillas, B. J. Votta, W. den Besten, K. Famm, L. Kruidenier, P. S. Carter, J. D. Harling, I. Churcher and C. M. Crews. Catalytic in vivo protein knockdown by small-molecule PROTACs. *Nat. Chem. Biol.* **2015**, *11*, 611-617.

9. C. Maniaci, A. Testa, X. Lucas W, K.H. Chan, W. Chen, D. J. Lamont, M. Zengerle and A. Ciulli. Structural basis of PROTAC cooperative recognition for selective protein degradation. *Nat. Chem. Biol.* **2017**, *13*, 514–521.
10. J. Hines, J. D. Gough, T. W. Corson and C. M. Crews. Posttranslational protein knockdown coupled to receptor tyrosine kinase activation with phosphoPROTACs. *Proc. Natl. Acad. Sci. U. S. A.* **2013**, *110*, 8942-8947.
11. G. M. Burslem, B. E. Smith, A. C. Lai, S. Jaime-Figueroa, D. C. McQuaid, D. P. Bondeson, M. Toure, H. Dong, Y. Qian, J. Wang, A. P. Crew, J. Hines and C. M. Crews. The advantages of targeted protein degradation over inhibition: an RTK case study. *Cell Chem. Biol.* **2018**, *25*, 67-77.
12. C. M. Robb, J. I. Contreras, S. Kour, M. A. Taylor, M. Abid, Y. A. Sonawane, M. Zahid, D. J. Murry, A. Natarajan and S. Rana. Chemically induced degradation of CDK9 by a proteolysis targeting chimera (PROTAC). *Chem. Comm.* **2017**, *53*, 7577-7580.
13. C. M. Olson, B. Jiang, M. A. Erb, Y. Liang, Z. M. Doctor, Z. Zhang, T. Zhang, N. Kwiatkowski, M. Boukhali, J. L. Green, W. Haas, T. Nomanbhoy, E. S. Fischer, R. A. Young, J. E. Bradner, G. E. Winter and N. S. Gray. Pharmacological perturbation of CDK9 using selective CDK9 inhibition or degradation. *Nat. Chem. Biol.* **2018**, *14*, 163-170.
14. H. T. Huang, D. Dobrovolsky, J. Paulk, G. Yang, E. L. Weisberg, Z. M. Doctor, D. L. Buckley, J. H. Cho, E. Ko, J. Jang, K. Shi, H. G.Choi, J. D. Griffin, Y. Li, S. P. Treon, E. S. Fischer, J. E. Bradner, L. Tan, and N. S. Gray. A chemoproteomic approach to query the degradable kinome using a multi-kinase degrader. *Cell Chem. Biol.* **2018**, *25*, 88-99.
15. H. Lebraud, D. J. Wright, C. N. Johnson, T. D. Heightman. Protein degradation by in-cell self-assembly of proteolysis targeting chimeras *ACS Cent. Sci.* **2016**, *2*, 927-934.

16. M. Zengerle, K.-H. Chan and A. Ciulli. Selective small molecule induced degradation of the BET bromodomain protein BRD4. *ACS Chem. Biol.* **2015**, *10*, 1770-1777.
17. K. Raina, J. Lu, Y. Qian, M. Altieri, D. Gordon, A. M. K. Rossi, J. Wang, X. Chen, H. Dong, K. Siu, J. D. Winkler, A. P. Crew, C. M. Crews and K. G. Coleman. PROTAC-induced BET protein degradation as a therapy for castration-resistant prostate cancer. *Proc. Natl. Acad. Sci. U. S. A.* **2016**, *113*, 7124-7129.
18. G. E. Winter, D. L. Buckley, J. Paulk, J. M. Roberts, A. Souza, S. Dhe-Paganon and J. E. Bradner. Phthalimide conjugation as a strategy for in vivo target protein degradation. *Science*, **2015**, *348*, 1376-1381.
19. J. Lu, Y. Qian, M. Altieri, H. Dong, J. Wang, K. Raina, J. Hines, J. D. Winkler, A. P. Crew, K. Coleman and C. M. Crews. Hijacking the E3 ubiquitin ligase cereblon to efficiently target BRD4. *Chem. Biol.* **2015**, *22*, 755-763.
20. D. Remillard, D. L. Buckley, J. Paulk, G. L. Brien, M. Sonnett, H.-S. Seo, S. Dastjerdi, M. Wühr, S. Dhe-Paganon, S. A. Armstrong and J. E. Bradner. Degradation of the BAF complex factor BRD9 by heterobifunctional ligands. *Angew. Chem. Int. Ed.* **2017**, *56*, 5738-5843.
21. R. J. Patch, L. L. Searle, A. J. Kim, D. De, X. Zhu, H. B. Askari, J. C. O'Neill, M. C. Abad, D. Rentzeperis, J. Liu, M. Kemmerer, L. Lin, J. Kasturi, J. G. Geisler, J. M. Lenhard, M. R. Player and M. D. Gaul. Identification of diaryl ether-based ligands for estrogen-related receptor α as potential antidiabetic agents. *J. Med. Chem.* **2011**, *54*, 788-808.
22. R. J. J. Deshaies. Protein degradation: prime time for PROTACs. *Nat. Chem. Biol.* **2015**, *11*, 634-635.
23. Y Li, J Yang, A Aguilar. Discovery of MD-224 as a first-in-class, highly potent, and efficacious proteolysis targeting chimera murine double minute 2 degrader capable of achieving complete and durable tumor regression. *J. Med. Chem.* **2018**, *62* 448-467.

24. W. McCoull, T. Cheung, E. Anderson, P. Barton, J. Burgess, K. Byth, Q. Cao, M. P. Castaldi, H. Chen, E. Chiarparin, R. J. Carbajo, E. Code, S. Cowan, P. R. Davey, A. D. Ferguson, S. Fillery, N. O. Fuller, N. Gao, D. Hargreaves, M. R. Howard, J. Hu, A. Kawatkar, P. D. Kemmitt, E. Leo, D. M. Molina, N. O'Connell, P. Petteruti, T. Rasmusson, P. Raubo, P. B. Rawlins, P. Ricchiuto, G. R. Robb, M. Schenone, M. J. Waring, M. Zinda, S. Fawell and D. M. Wilson. Development of a novel B-cell lymphoma 6 (BCL6) PROTAC to provide insight into small molecule targeting of BCL6. *ACS Chem. Biol.* **2018**, *13*, 3131-3141.

25. J. W. Papatzimas, E. Gorobets, R. Maity, M. I. Muniyat, J. L. MacCallum, P. Neri, N. J. Bahlis, and D. J. Derksen. From inhibition to degradation: targeting the antiapoptotic protein myeloid cell leukemia 1 (MCL1). *J. Med. Chem.* **2019**, *62*, 5522-5540.

26. V. Azzarito, K. Long, N. S. Murphy and A. J. Wilson. Inhibition of α-helix-mediated protein–protein interactions using designed molecules. *Nat. Chem.* **2013**, *5*, 161-173.

27. M. Pelay-Gimeno, A. Glas, O. Koch and T. N. Grossmann. Structure-based design of inhibitors of protein-protein interactions: mimicking peptide binding epitopes. *Angew. Chem. Int. Ed.* **2015**, *54*, 8896-8927.

28. L. G. Milroy, T. N. Grossmann, S. Hennig, L. Brunsveld and C. Ottmann. Modulators of protein-protein interactions. *Chem. Rev.* **2014**, *114*, 4695-4728.

29. D. P. Ryan and J. M. Matthews. Protein-protein interactions in human disease. *Curr. Opin. Struct. Biol.*, 2005, **15**, 441-446.

30. A. Aouacheria, V. Rech de Laval, C. Combet and J. M. Hardwick. Evolution of Bcl-2 homology motifs: homology versus homoplasy. *Trends Cell. Biol.* 2013, **23**, 103-111.

31. A. Aouacheria, C. Combet, P. Tompa and J. M. Hardwick. Redefining the BH3 death domain as a short linear motif. *Trends Biochem. Sci*. **2015**, *40*, 736-748.

32. F. Pentimalli. BCL2: a 30-year tale of life, death and much more to come. *Cell Death. Differ.* **2018**, *25*, 7-9.

33. J. L. Yap, L. Chen, M. E. Lanning and S. Fletcher. Expanding the Cancer Arsenal with Targeted Therapies: Disarmament of the antiapoptotic Bcl-2 proteins by small molecules: miniperspective. *J. Med. Chem.* **2017**, *60*, 821-838.

34. M. S. Gadd, A. Testa, X. Lucas, K. H. Chan, W. Chen, D. J. Lamont, M. Zengerle and A. Ciulli. Structural basis of PROTAC cooperative recognition for selective protein degradation. *Nat. Chem. Biol.* **2017**, *13*, 514-521.

35. D. P. Bondeson, B. E. Smith, G. M. Burslem, A. D. Buhimschi, J. Hines, S. Jaime-Figueroa, J. Wang, B. D. Hamman, A. Ishchenko and C. M. Crews. Lessons in PROTAC design from selective degradation with a promiscuous warhead. *Cell Chem. Biol.* **2018**, *25*, 78-87.

36. Z. Zhang, G. Wu, F. Xie, T. Song and X. Chang. 3-Thiomorpholin-8-oxo-8 H-acenaphtho [1, 2-b] pyrrole-9-carbonitrile (S1) based molecules as potent, dual inhibitors of B-cell lymphoma 2 (Bcl-2) and myeloid cell leukemia sequence 1 (Mcl-1): structure-based design and structure-activity relationship studies. *J. Med. Chem.* **2011**, *54*, 1101-1105.

37. T. Song, Q. Chen, X. Li, G. Chai and Z. Zhang. Correction to 3-Thiomorpholin-8-oxo-8 H-acenaphtho [1, 2-b] pyrrole-9-carbonitrile (S1) based molecules as potent, dual inhibitors of B-cell lymphoma 2 (Bcl-2) and myeloid cell leukemia sequence 1 (Mcl-1): structure-based design and structure-activity relationship studies. *J. Med. Chem.* **2013**, *56*, 9366-9367.

38. T. Song, Z. Wang, F. Ji, Y. Feng, Y. Fan, G. Chai, X. Li, Z. Li and Z. Zhang. Deactivation of Mcl-1 by dual-function small-molecule inhibitors targeting the Bcl-2 homology 3 domain and facilitating Mcl-1 ubiquitination. *Angew. Chem. Int. Ed.* **2016**, *55*, 14250-14256.

39. Z. Wang, Z. Guo, T. Song, X. Zhang, N. He, P. Liu, P. Wang and Z. Zhang. Proteome-wide identification of on-and off-targets of Bcl-2 inhibitors in native

biological systems by using affinity-based probes (AfBPs). *Chembiochem* **2018**, *19*, 2312-2320.

40. C. Steinebach, S. Lindner, N. D. Udeshi, D. C. Mani, H. Kehm, S. Köpff, S. A. Carr, M. Gütschow and J. Krönke. Homo-PROTACs for the chemical knockdown of cereblon. *ACS Chem. Biol.* **2018**, *13*, 2771-2782.
41. Z. Wang, T. Song, Y. Feng, Z. Guo, Y. Fan, W. Xu, L. Liu, A. Wang and Z. Zhang. Bcl-2/MDM2 dual Inhibitors based on universal pyramid-like α-helical mimetics. *J. Med. Chem.* **2016**, *59*, 3152-3162.
42. E. Fire, S. V. Gulla, R. A. Grant and A. E. Keating. Mcl-1-Bim complexes accommodate surprising point mutations via minor structural changes. *Protein Sci.* **2010**, *19*, 507-519.
43. B. Ku, C. Y. Liang, J. U. Jung and B. H. Oh. Evidence that inhibition of BAX activation by BCL-2 involves its tight and preferential interaction with the BH3 domain of BAX. *Cell Res.*, **2011**, *21*, 627-641.
44. P. P. Chamberlain, A. Lopez-Girona, K. Miller, G. Carmel, B. Pagarigan, B. Chie-Leon, E. Rychak, L. G. Corral, Y. J. Ren, M. Wang, M. Riley, S. L. Delker, T. Ito, H. Ando, T. Mori, Y. Hirano, H. Handa, T. Hakoshima, T. O. Daniel and B. E. Cathers. Structure of the human cereblon-DDB1-lenalidomide complex reveals basis for responsiveness to thalidomide analogs. *Nat. Struct. Mol. Biol.* **2014**, *21*, 803-809.
45. M. Bruncko, L. Wang, G. S. Sheppard, D. C. Phillips, S. K. Tahir, J. Xue, S. Erickson, S. Fidanze, E. Fry, L. Hasvold, G. J. Jenkins, S. Jin, R. A. Judge, P. J. Kovar, D. Madar, P. Nimmer, C. Park, A. M. Petros, S. H. Rosenberg, M. L. Smith, X. Song, C. Sun, Z. F. Tao, X. Wang, Y. Xiao, H. Zhang, C. Tse, J. D. Leverson, S. W. Elmore and A. J. Souers. Structure-guided design of a series of MCL-1 inhibitors with high affinity and selectivity. *J. Med. Chem.* **2015**, *58*, 2180-2194.

TOC

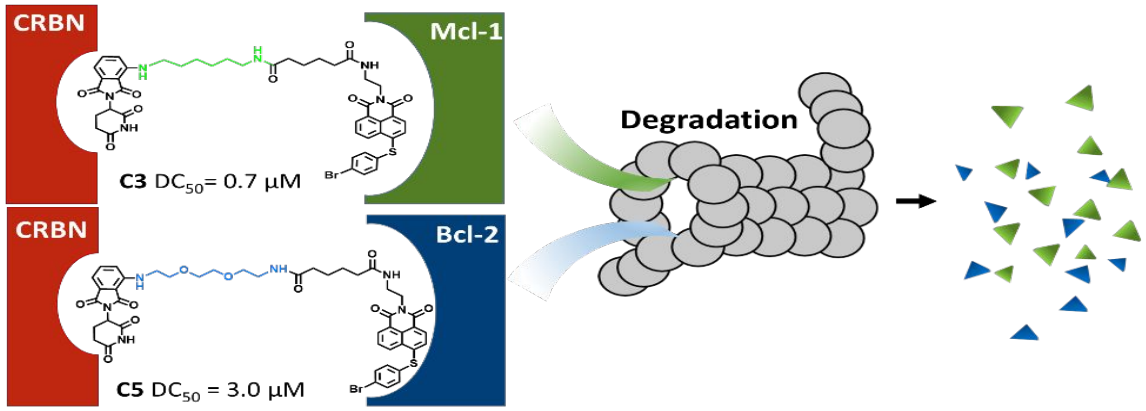

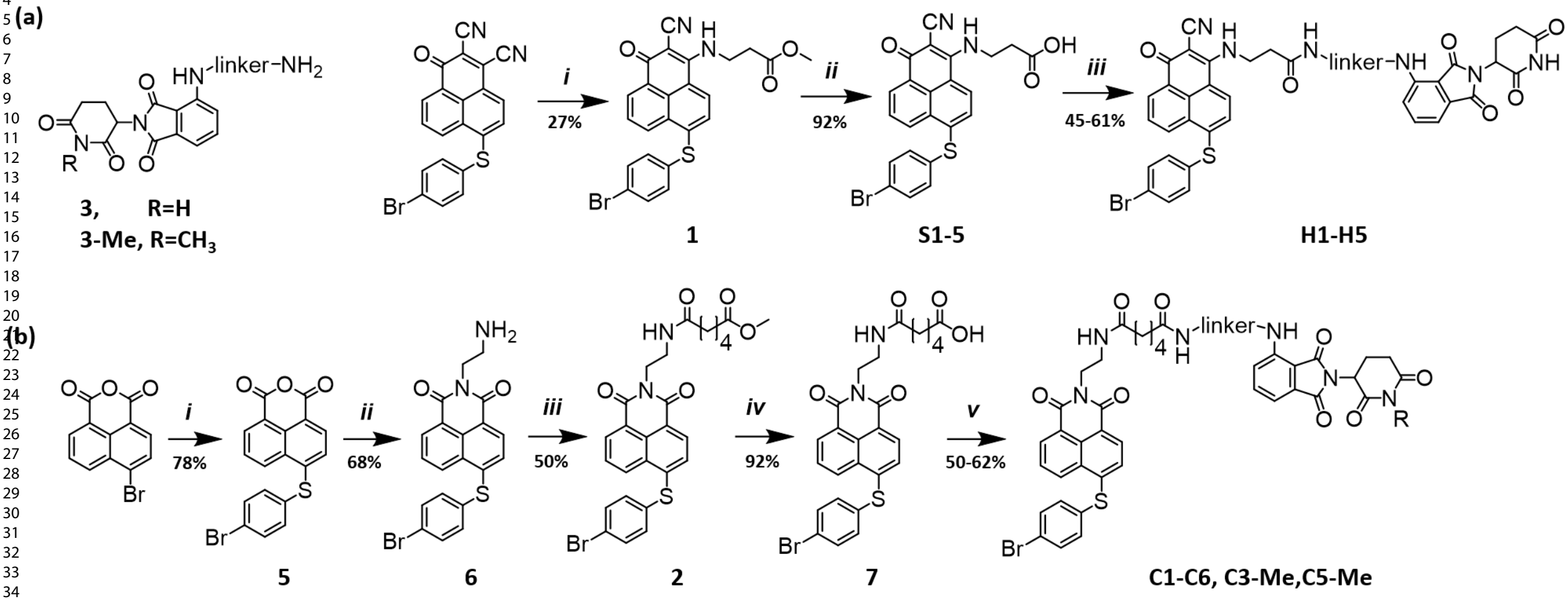
(a)
HN-linker-NH2
3, R=H
3-Me, R=CH3
i
27%
1
ii
92%
S1-5
iii
45-61%
H1-H5
(b)
i
78%
5
ii
68%
6
iii
50%
2
iv
92%
7
v
50-62%
C1-C6, C3-Me,C5-Me

(a)

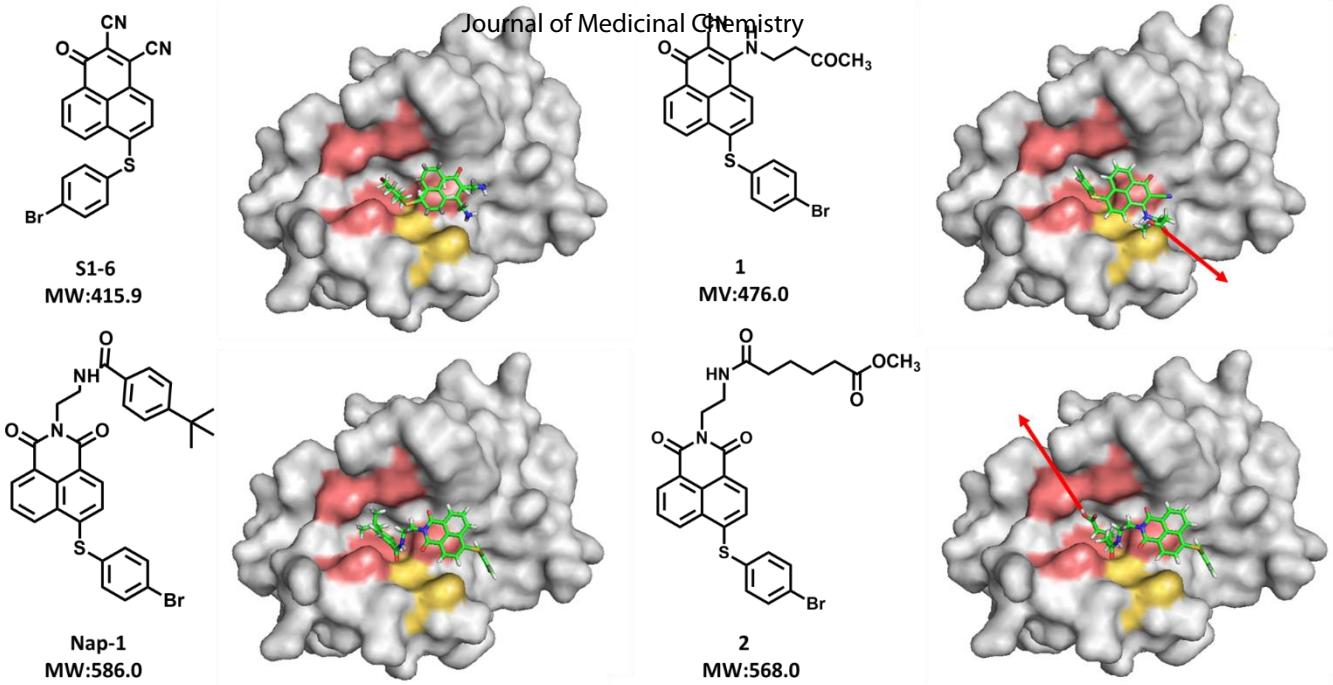

(b)

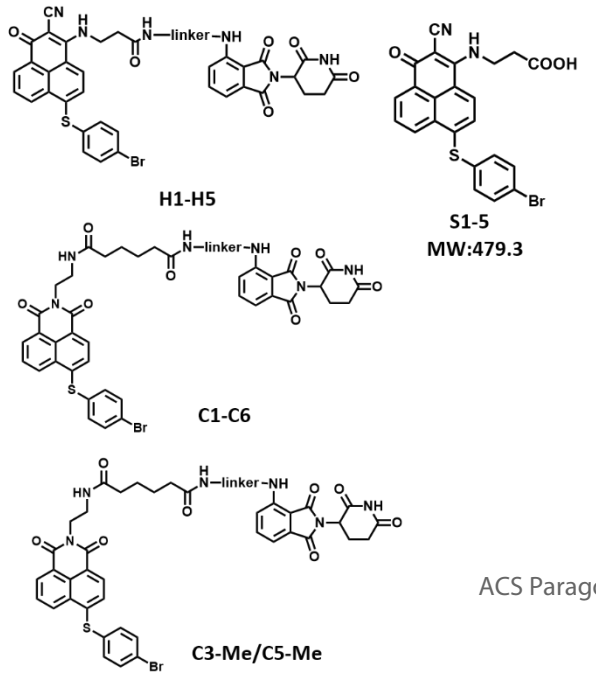

No.	MW	Linker
C1	852.1	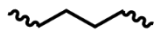
H1	777.6	
C2	880.1	
H2	805.7	
C3	908.2	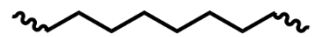
H3	833.7	
C4	1021.3	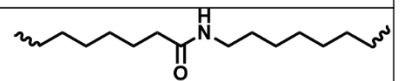
H4	945.2	
C5	940.2	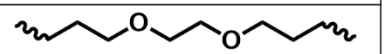
H5	864.1	
C6	936.3	
C3-Me	922.2	
C5-Me	954.2	

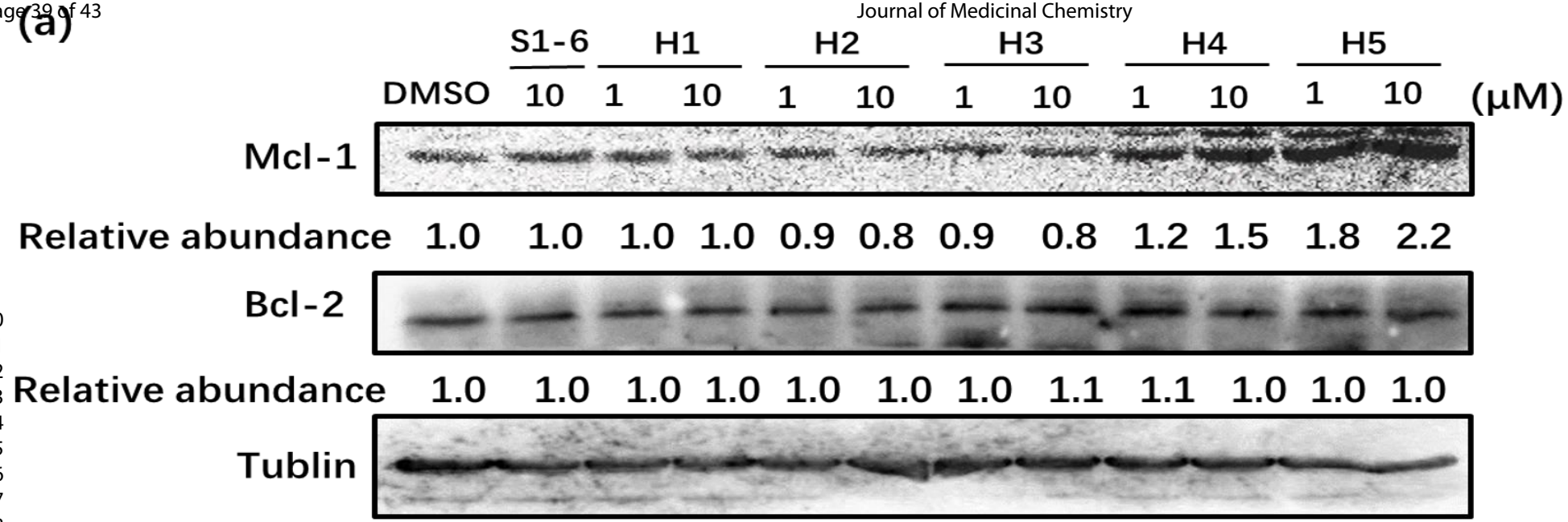

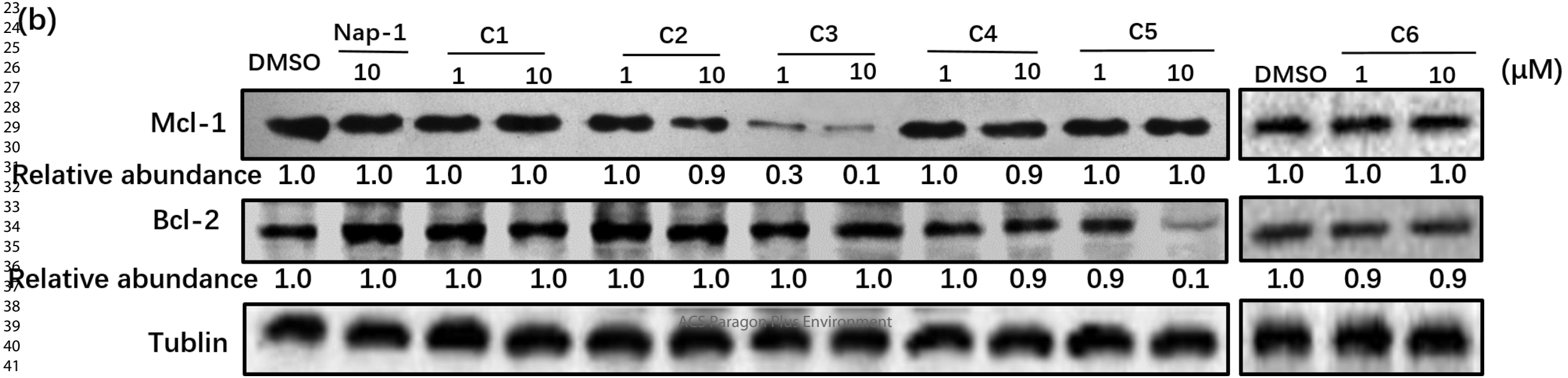

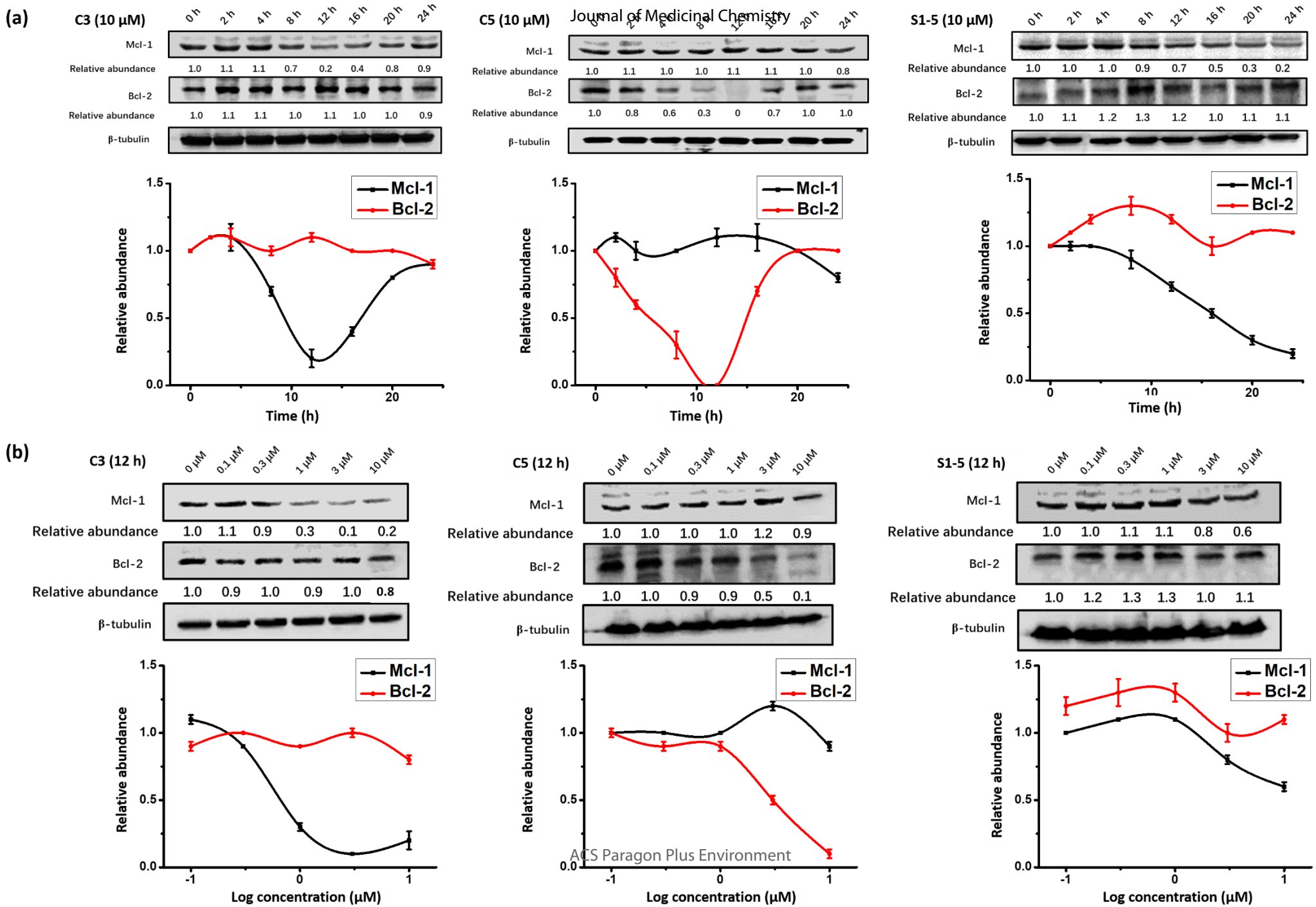

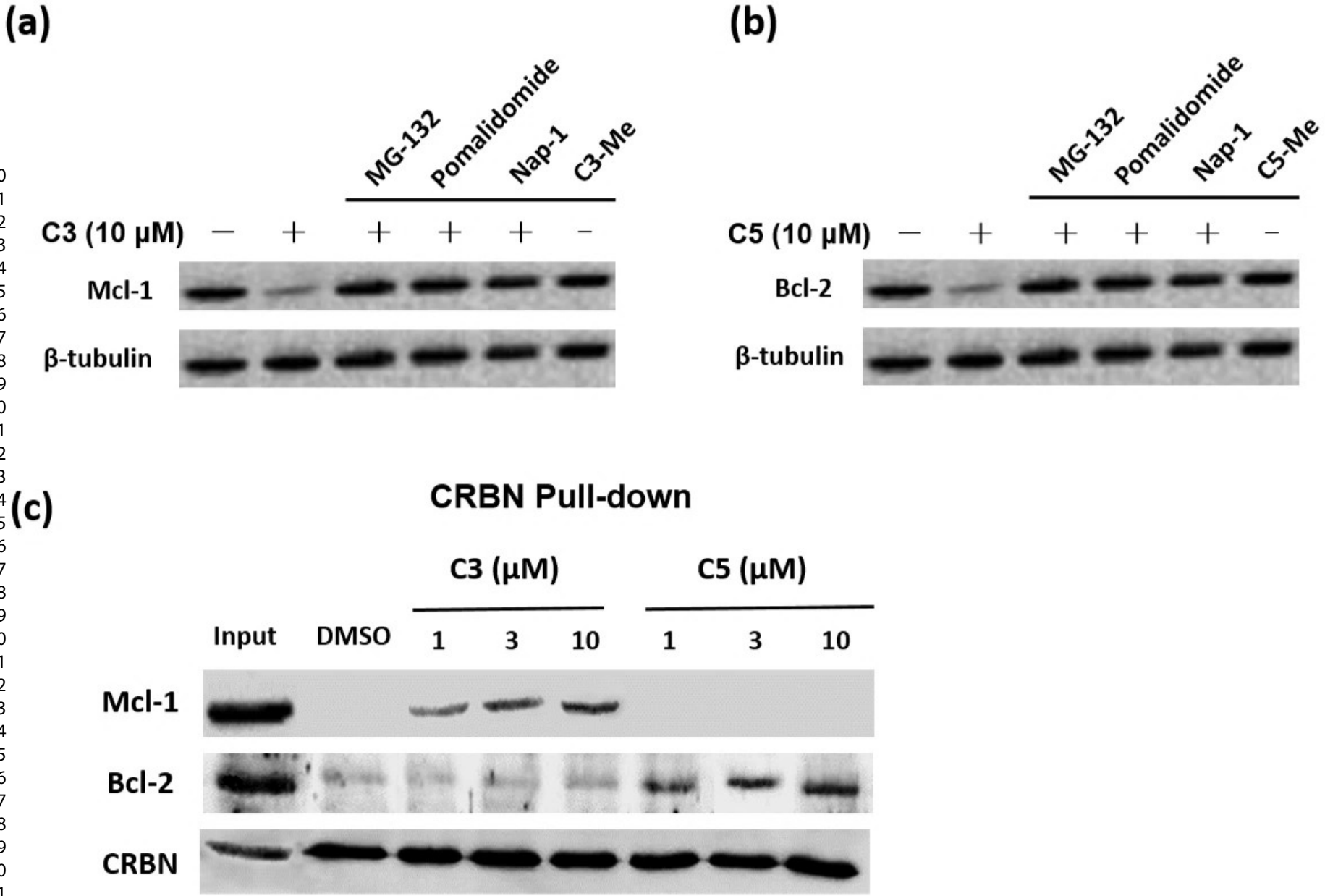
(a)
MG-132
Pomalidomide
Nap-1
C3-Me
C3 (10 μM)
Mcl-1
β-tubulin
(b)
MG-132
Pomalidomide
Nap-1
C5-Me
C5 (10 μM)
Bcl-2
β-tubulin
(c)
CRBN Pull-down
C3 (μM)
C5 (μM)
Input
DMSO
1
3
10
1
3
10
Mcl-1
Bcl-2
CRBN

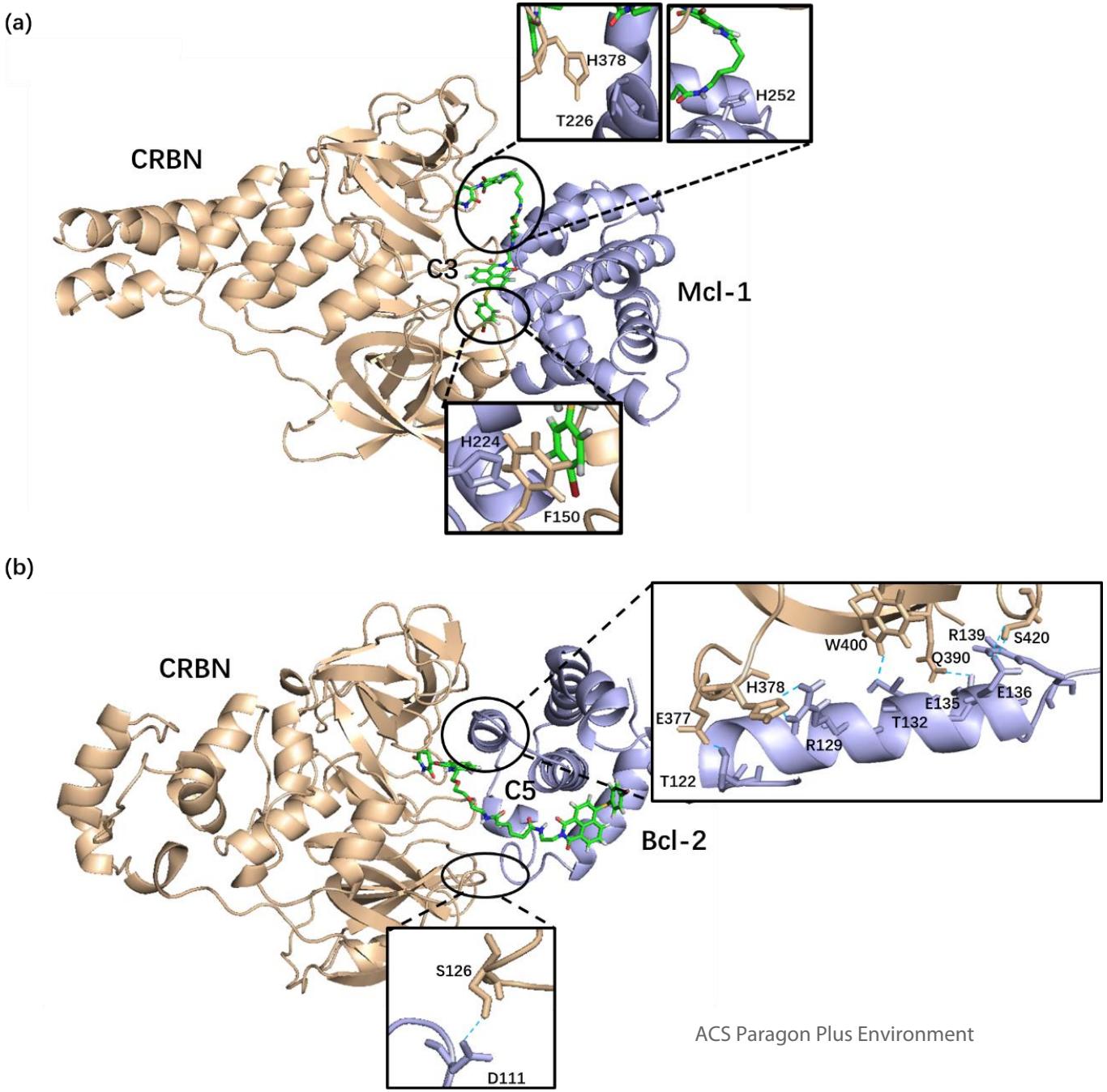
(a)
CRBN
C3
Mcl-1
H378
T226
H252
H224
F150
(b)
CRBN
C5
Bcl-2
W400
R139
S420
Q390
H378
E377
E135
E136
T132
R129
T122
S126
D111

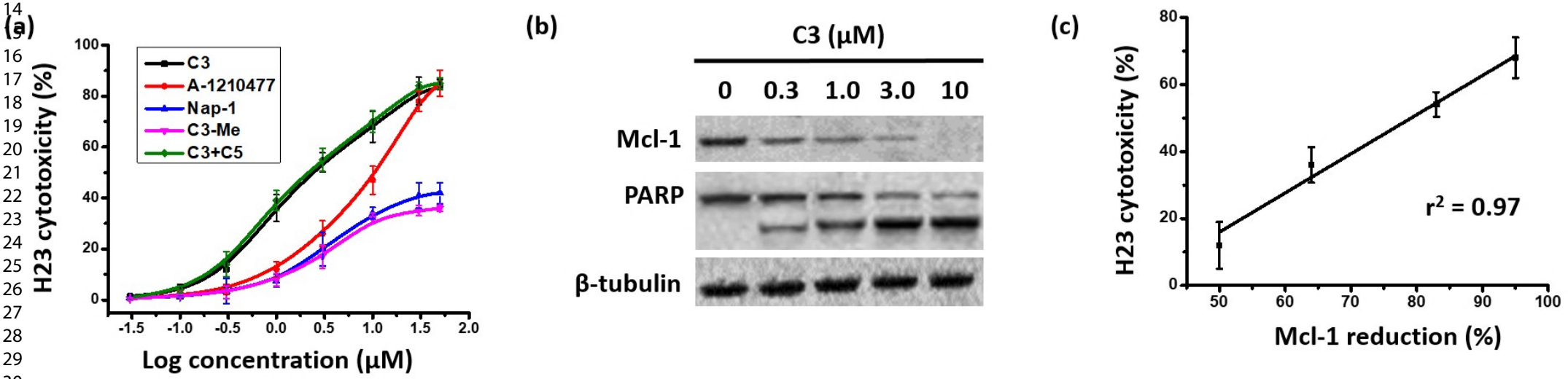
(a)
H23 cytotoxicity (%)
Log concentration (μM)
C3
A-1210477
Nap-1
C3-Me
C3+C5
(b)
C3 (μM)
0 0.3 1.0 3.0 10
Mcl-1
PARP
β-tubulin
(c)
H23 cytotoxicity (%)
Mcl-1 reduction (%)
r² = 0.97